Applied Catalysis A, General 697 (2025) 120196

Contents lists available at ScienceDirect

Applied Catalysis A, General

journal homepage: www.elsevier.com/locate/apcata

Use of a 416B-type central-hybrid experimental design to evaluate the synthesis conditions of TiO_2/biochar composites on the solid-state photocatalytic degradation of polypropylene-plastic films

Deyler Castilla-Caballero [a,b,c,*], Astrid Medina-Guerrero [c], Aracely Hernandez-Ramirez [d], Sofia Vazquez-Rodriguez [e], José Colina-Márquez [f], Fiderman Machuca Martínez [b], Juan Barraza-Burgos [b], Aicardo Roa-Espinosa [g], Sundaram Gunasekaran [h,**]

[a] Environmental Engineering and Chemical Engineering Programs, Universidad Tecnológica de Bolívar, Parque Industrial y Tecnológico Carlos, Vélez Pombo km 1 Vía Turbaco, Cartagena, Colombia
[b] Escuela de Ingenieria Química, Universidad del Valle, Cali 760026, Colombia
[c] School of Engineering, Architecture & Design, Universidad Tecnológica de Bolívar, Parque Industrial y Tecnológico Carlos, Vélez Pombo km 1 Vía Turbaco, Cartagena, Colombia
[d] Facultad de Ciencias Químicas, Universidad Autónoma de Nuevo León, Ave. Universidad S/N, Cd. Universitaria, C.P. 66455, San Nicolás de los Garza, NL, Mexico
[e] Facultad de Ingeniería Mecánica y Eléctrica, Universidad Autónoma de Nuevo León, Pedro de Alba S/N, Cd. Universitaria, San Nicolás de los Garza, NL 66455, Mexico
[f] Chemical Engineering Program, Universidad de Cartagena, Av. El Consulado 48-152, Cartagena A.A. 130001, Colombia
[g] Soil Net LLC, 560 Enterprise Ave, Belleville, WI 53508, USA
[h] Department of Biological Systems Engineering, University of Wisconsin, Madison, WI 53706, USA

ARTICLE INFO

Keywords:
Solid-state photocatalysis
TiO_2/biochar
Polypropylene
Plastic pollution
416B-type central-hybrid experimental design

ABSTRACT

This study presents an innovative application of solid-state photocatalysis using environmentally friendly TiO_2/biochar composites to degrade polypropylene (PP) films and reduce plastic pollution. Biochar, derived from coconut shells via controlled pyrolysis, was combined with TiO_2 to enhance photocatalytic activity. A 416B-type Central-Hybrid Experimental Design was used to optimize synthesis parameters, revealing that biochar produced at 280°C with 4.1 % v/v oxygen and a TiO_2/biochar weight ratio of 1.5 yields the best results. After 25 days of UV irradiation, films incorporated with TiO_2/biochar composites exhibited an 8.7 % weight loss and a carbonyl index of 11.4—significantly surpassing pristine PP films. These findings demonstrate the potential of biochar as a sustainable solution to reduce nanotoxicity while boosting polymer degradation efficiency. This work contributes to the development of eco-friendly materials for mitigating plastic waste challenges.

1. Introduction

Plastics are petroleum-derived polymers that have been widely used because they possess remarkable physical and chemical properties, such as water and corrosion resistance, chemical stability, ease of molding, and good thermal and electrical insulation properties [1,2]. They also possess other attractive characteristics such as ease of production, versatility, and low purchase price [2]. Despite the global tendency to reduce the use of these materials, which is motivated by reasonable environmental concerns, their unique properties have hindered their complete substitution so far. Since the middle of the 20th century, hundreds of millions of tons of polymer products have been produced on the planet [2–5], while in 2020, global production was 367 million metric tons [6]. During the COVID-19 pandemic, the demand for plastic-derived products such as facemasks rose sharply [7], which also implied an increased production of the polymers that comprise them (i.e., PP and PE [7]). However, despite the advantages of plastics in everyday life, the adverse effects of their improper disposal on the environment are becoming increasingly evident. In the case of plastics used in packaging and containers [8,9], it has been reported that 40 % eventually ended up in landfills, 32 % were dumped into the environment, contaminating soils and oceans, while 28 % was collected for further use, either in incineration (for energy production) or for

* Corresponding author at: Environmental Engineering and Chemical Engineering Programs, Universidad Tecnológica de Bolívar, Parque Industrial y Tecnológico Carlos, Vélez Pombo km 1 Vía Turbaco, Cartagena, Colombia.
** Corresponding author.
E-mail addresses: dcastilla@utb.edu.co (D. Castilla-Caballero), guna@wisc.edu (S. Gunasekaran).

https://doi.org/10.1016/j.apcata.2025.120196
Received 10 December 2024; Received in revised form 28 January 2025; Accepted 27 February 2025
Available online 6 March 2025

Nomenclature

B-T	TiO_2/biochar composites
CI	Carbonyl Index
HDPE or rHDPE	High-density polyethylene or recycled HDPE
LDPE	Low-density polyethylene
PE	Polyethylene
HI	Hydroxyl index
i-t	Current vs time
$\%O_2$	Oxygen percentage in the pyrolysis reaction
OCP	Open circuit potential
PL	Photoluminescence
PP	Polypropylene
PVC	Poly (vinyl chloride)
T/B, Ti/B or TiO_2/biochar	Mass ratio of TiO_2 and biochar used for their coupling
Tcal	Calcination temperature used for coupling TiO_2 with biochars
Tpyrol	Pyrolysis temperature

recycling. It is estimated that only 2 % were recycled to obtain products with similar characteristics to the original ones, while 8 % was destined for "cascade" recycling. Currently, the generation of plastic solid waste represents a significant problem due to factors such as: the large land occupation required for the disposal of these wastes; their low degradation rate [10], which implies their permanence up to hundreds of years in the disposal site [9]; the contamination of water, soil, flora and fauna that can be caused by their inadequate disposal [2,11,12]; problems in the operation of landfills because these materials are difficult to treat and stabilize geotechnically [11], since plastics are bulky materials that hinder landfill compaction and delay the degradation of other organic materials [13]; and finally, the landscape impact when they are abandoned in the open air [11]. Polyolefin-based (i.e., PP or PE) plastic bags currently represent another type of environmental threat because their incorrect disposal harms aquatic and terrestrial biota [14] [15] and may promote the appearance of human diseases [16]. Many countries have banned plastic bags to reduce their adverse effects [17–19]. However, since packaging, containers, facemasks, and other polyolefin-based products have proven to be necessary for the daily activities of global society; and, taking into account that their prohibition could generate traumas in these activities due to the reliance of people and the industrial sector on their use, it is necessary to develop products that meet the same need, but that do not generate the same negative impacts.

It is necessary to mention that the common methods for disposing of and treating polyolefin waste include incineration, recycling, and sanitary landfills. Incineration produces toxic compounds, acid gases, and heavy metals, harming the environment and health [20–22]. Recycling is not yet an economically viable option due to high operating costs [2, 21]. Finally, landfills are not a sustainable alternative because after their capacity has been filled, they cannot be reused, so they should be considered the last option. Biodegradation is also under heavy study, but its large-scale applicability is not yet clear [23], and the current biodegradable polymers do not possess good mechanical properties as the conventional plastics do [24,25]. However, research is being addressed to improve these properties through biodegradable polymer blending [25].

On the other hand, TiO_2 photocatalysis is effective for the treating hazardous and poorly biodegradable substances [26–29]. Due to its non-selectivity, low chemical toxicity, and operation at a relatively low cost, this advanced oxidation process is as a possible alternative or aid to common decontamination treatments. Aeroxide-P25 TiO_2 is the commercial brand of TiO_2 employed in most of the works using photocatalysis. This is a mixture of the crystallographic phases of TiO_2 Anatase (80 %) and Rutile (20 %) that due to its synergistic effects has usually shown remarkable optoelectronic properties, greater than those of other types of TiO_2 [20,30]. Even though most publications on photocatalysis are focused on treating contaminants in aqueous and gaseous media, there have been relatively few reports on solid-state degradation, most related to plastic degradation. Recently, Castilla-Caballero et al. [31] presented a review highlighting the main milestones in applying solid-state photocatalysis for plastics abatement. There, some reports showing promising results on the degradation of PP, PE, and PVC are discussed. However, given the chemical nature of polyolefins and TiO_2, the agglomeration of the semiconductor within the polymeric network hinders the degradation process. This is because it decreases the interfacial area between the polymer to be degraded and TiO_2, as well as accelerates whitening, which decreases the penetration of light -that promote photocatalysis- into the material [20,32].

Furthermore, the hydrophobic nature of polyolefins, along with accentuating its low biodegradability rate, dramatically inhibits the photocatalytic activity of the semiconductor. The reason for this behavior is that the scarcity of water molecules in the polymeric network limits the occurrence of the strong oxidizing species (such as hydroxyl radicals) responsible for destroying the contaminants through photocatalysis. Besides, TiO_2, despite being the most employed photocatalyst due to its notable properties, exhibits an elevated rate of recombination of the photogenerated electron-hole pairs and a reduced utilization of the solar spectrum, which hinders greater exploitation of solar photocatalysis. Additionally, due to its reduced size, TiO_2 shows a nanotoxicity risk to living beings if released into the environment because it can penetrate their cells. Furthermore, there are reports on using aqueous-phase photocatalysis to transform plastic wastes into added-value products [33–36], but in those cases, the required water may be polluted due to the aggressive reagents needed for this application.

The potential benefits of Aeroxide P25 TiO_2/biochar composites in reducing the recombination rate of electron-hole pairs and the semiconductor band gap are remarkable [37]. Further, it has been reported that biochar can improve the mechanical properties (tensile modulus, flexural strength, and/or stiffness) of specific polymers such as polypropylene, polylactic acid, epoxy resin and others [38], and rHDPE [39] when employed as a filling agent, and even reduce their environmental impact [39]. They are advantageous compared to other biofillers (wood, jute, flax fiber) because they possess high thermal stability [38]. Along with this, it has been reported that biochars can exhibit compatibility with petrochemical related plastics, showing a low tendency to form dispersed phases when mixed [38]. In addition, biochar pores can serve as mechanical attachment points that allow polymers to embed in them [38]. Also, due to the high porosity and the presence of hydrophilic functional groups in their structure that may form during pyrolysis, biochars may have the ability to absorb surrounding moisture [40,41], which would be beneficial to generate hydroxyl radicals which are relevant for the solid-state abatement of plastics.

Additionally, because biochar can be obtained from many types of waste, the storage capacity of landfills could be alleviated by transforming these wastes into added-value materials. Moreover, their production does not compete with food crops, as would be the case with other types of biological additives. In this work, coconut shells were used to produce biochar because they are a typical waste from Colombian agro-industries. In addition, the nanotoxicity effect associated with TiO_2 could be prevented by using biochar microparticles as titania support. As a result, in this work, a novel strategy is presented for degrading PP-based films through solid-state photocatalysis using TiO_2 modified with biochars synthesized through the pyrolysis of coconut-shell wastes. The purpose is, along with contributing to environmental science research, to expand the current knowledge of solid-state photocatalysis, giving insight into how the synthesis conditions of the novel TiO_2/biochar catalyst employed (temperature and O_2 content of

pyrolysis, TiO_2/biochar ratio and calcination temperature) impact the reaction rate of the solid-state elimination of PP by using a robust 416B-type Central-Hybrid Experimental Design. This kind of experimental design is attractive when an elevated number of factors are to be analyzed because they have a reduced (almost minimal) number of experiments, keeping a degree of orthogonality (like the well-known Central Compound Designs), which allow more accurate estimation of the effects, and approximate rotatability, to ensure the quality of predictions [42,43]. With it, the balance between statistical rigor and experimental efficiency is a plus. Also, this type of design permits the analysis of each factor's effect on the response variable individually and their interactions.

2. Materials and methods

2.1. Materials

Biochars were synthesized by the slow pyrolysis (temperature range: 280 −420 °C, reaction time: 1 h, heating rate: 10°C/min) of coconut shell wastes obtained from the Colombian Pacific Coast, employing an atmosphere consisting of N_2 and minimal or null amounts of O_2 (0−5 % v/v). The pyrolysis was performed in six parallel cylindrical ceramic reactors with lid that were placed inside a muffle furnace (Multi-purpose muffle from Terrigeno). The reactors were initially loaded with ~25 g of ground coconut shells (particle size less than 250 μm) and fed with a continuous flow of 4210 ml/min of the N_2/O_2 stream during the carbonization process. A detailed description of biochar synthesis is indicated in ref. [44]. Aeroxide TiO_2 P25 from Evonik (~ 80 % anatase and 20 % rutile, average diameter of the primary particles of 21 nm, specific surface area of 50 $m^2\ g^{-1}$ and density of ~ 4 g/cm^3 [45]) was used for the experiments. The coupling of TiO_2 and biochars for obtaining the TiO_2/biochar composites that were further used to fabricate the PP-based nanocomposites was made by using a facile wet impregnation/calcination method that comprises mechanical stirring of biochar and sonicated TiO_2 for four hours in distillated water. Next, this mixture was centrifugated at 10000 rpm for 20 min to remove most of the water. Then, the material was dried at 80°C overnight and calcinated from 30°C to 800 °C in an N_2 atmosphere for 30 min to produce the TiO_2/biochar composites. The calcination was conducted in a tubular furnace (GSL-1100X) using combustion-boat crucibles as containers. This procedure is described in Schematic 1 and further explained in ref [37], along with the presentation of a comprehensive characterization of the TiO_2/biochar composites which included XRD, XPS, FT-IR, UV-Vis DRS, PL, SEM, BET surface area, and electrochemical analysis, some of which are summarized in Table S 1. Pro-fax SG702 polypropylene in pellets (LyondellBasell) was used to manufacture pure and modified PP-based films. This compound is a high-impact polypropylene copolymer with a relative density of 0.9 g/cm^3 (23°C, ASTM D792) and a melt flow index (230°C/2.16 kg) of 18.0 g/10 min (ASTM D1238) [46].

2.2. Synthesis and characterization of the PP-TiO_2/Biochar composites and films

The preparation of the PP-TiO_2/Biochar composites was made through a laboratory scale extruder (LME 120 from Dynisco) as follows: initially, the TiO_2/biochar material obtained in the impregnation stage was manually mixed with PP pellets and placed in a vessel. For each extrusion run, 10 g of PP and 100 mg of TiO_2/Biochar were used, so that the mass percentage of the TiO_2/Biochar load in the PP-TiO_2/Biochar composite was 1.0 wt%. Then, the pre-mix of PP with TiO_2/Biochar was carefully fed into the extruder hopper, where the extrudate began to flow out continuously. The head and rotor temperature of the extruder and the rotor speed were previously fixed at 183 °C and 162 °C, respectively, whereas the rotor speed was set at 44.4 rpm. Furthermore, for the correct operation of the extruder, a water flow of approximately 200 cm^3/min was provided in the cooling jacket of the feed hopper. For this purpose, a Wheaton-Omnispense peristaltic pump was used, operating at 145 rpm. Due to the better homogeneity of the resulting PP-TiO_2/biochar composite, the last protruding half of the extrudate was selected, chopped, and collected in resealable bags. Also, to evaluate the photolytic and the photocatalytic degradation of PP using only TiO_2 (and not biochar, nor TiO_2/biochar), extrudate blanks of virgin PP and PP with TiO_2 alone (using TiO_2 loads of 0.1, 0.5 and 1.0 wt%) were synthesized according to the steps mentioned before. Next, the chopped extrudates were hot-pressed using a Carver press operating at 5000 lbf and a temperature of 175°C in both plates, which allowed to obtain thick films (~ 0.1 mm, measured with an electron micrometer, SHARS 0–1 "). Hot-pressing was performed in batches for one minute using 700 mg of extrudate and subsequently, the films produced were allowed to cool down in air for 30 s. These films were then cut into 1.4 cm x 3.9 cm pieces for being submitted to photodegradation tests.

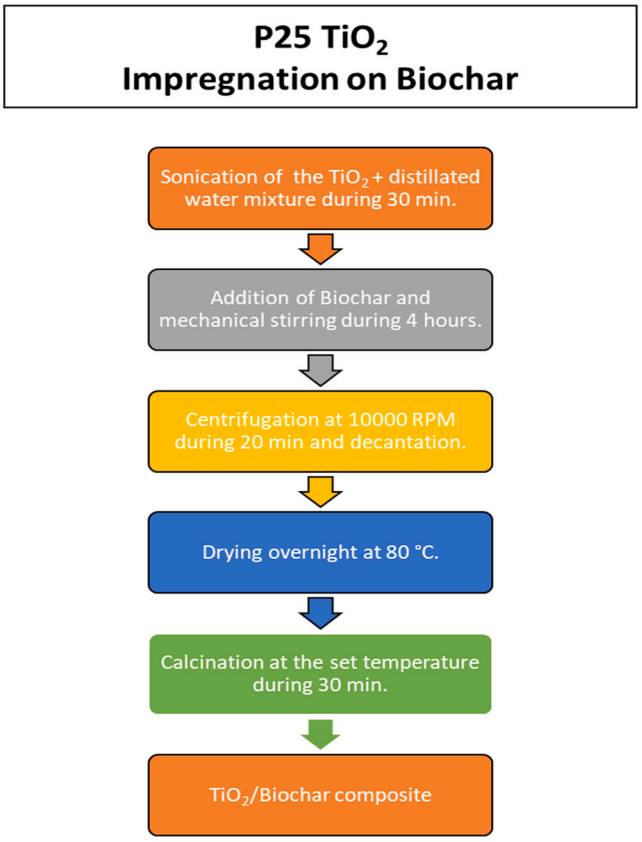

Schematic 1. Wet impregnation method for producing the TiO_2/Biochar composites.

The amount of TiO_2 present in the plastic films was determined indirectly by detecting the Ti elemental content of the samples through the X-ray fluorescence technique (S1 TITAN - Handheld XRF Analyzer from Bruker) by comparing the amounts of titanium present in the virgin samples (PP films) with those found in the PP-TiO_2/biochar and PP-TiO_2 based materials. The detection limits of the instrument are 100 ppm for one minute of measuring time and decrease to 25 ppm after four minutes of measuring time, according to the user's (Soil Net) experience. In all cases, the measuring time was approximately one minute, however. On the other hand, a comprehensive characterization of the TiO_2/biochar composite alone is presented in ref. [36].

2.3. Solid-state photocatalytic degradation of PP

The photodegradation tests were carried out in a dark room using two 15 W black-light UV lamps (F15T8 / BLB) with an emission peak of 368 nm and maximum irradiance of 1.75 x 10^{-5} W/cm^2 nm, which were

located ~7 cm above the films (See Fig. 1). The emission spectrum and spectral power of the lamps can be found on the supplier's (GE Lighting) website. The photodegradation experiment lasted 25 days, during which the change in the mass of the films was measured using a digital analytical balance (AG245 from Mettler Toledo, 0.1 mg sensitivity). Then, the weight loss of the films was calculated according to Eq. (1), where m_0 represents the initial weight of the films and m_f is the weight of the films after the photodegradation process:

$$\%\text{Weight loss} = 100 * \frac{m_0 - m_f}{m_0} \quad (1)$$

On the other hand, the oxidation of the films was measured indirectly by detecting the evolution of the carbonyl groups through FTIR spectroscopy using a Spectrum 100 apparatus from PerkinElmer. This allowed the calculation of the carbonyl index (CI, see Eq. (2)), stated as the ratio between the area of the carbonyl absorption band, A_C (1700 – 1800 cm^{-1}), and the area of a reference band, A_R, which remains chemically stable during the process of aging. In this case, the C–H stretch band was selected as the reference band, whose area was estimated in the 2700 –2750 cm^{-1} range, having a peak around 2720 cm^{-1} [20,47,48].

$$\text{Carbonyl Index} = \frac{A_C}{A_R} \quad (2)$$

Similarly, the hydroxyl index (HI) was calculated according to Eq. (3). This index has also been employed in the evaluation of the photooxidation of polyolefins [48]. It is defined as the ratio between the area of the absorption band of the hydroxyl groups, A_{OH} (3200 – 3600 cm^{-1}), and the area of the reference band, A_R, which is the same one defined earlier.

$$\text{Hydroxyl Index} = \frac{A_{OH}}{A_R} \quad (3)$$

2.4. Statistical optimization analysis

The degradation of PP films was analyzed with a 416B-type central-hybrid experimental design [42,49] coupled with the response surface methodology. The hybrid experimental designs are attractive when an elevated number of factors are to be analyzed because they have a reduced (almost minimal) number of experiments, a degree of orthogonality like central compound designs, which allow more accurate estimation of the effects, and approximate rotatability, to ensure the quality of predictions [42,50]. This kind of design is desirable for analyzing the effect of each factor on the response variable, both individually and in their interactions. For better clarity, in the title of the experimental design (416-B) the first digit indicates the number of the variables, the next two digits are the number of points, and the letter differentiates the table design from others of the same size [42]. Due to our objective is analyzing the best combination of raw material pretreatment to produce a photodegradable polymeric matrix, degradation percentage was considered as the response variable and, the effect of the following 4 factors on the photodegradation of the films was evaluated: the temperature and oxygen content (%v/v) in the pyrolysis reactor where biochars were synthesized, the TiO_2/biochar ratio in the impregnation process employed to fabricate the TiO_2/biochar composites, and the calcination temperature of the PP-TiO_2/Biochar composites (see Table 1) that were used with PP to produce the plastic films. The temperatures and percentages of oxygen in the pyrolysis used in the experimental design were detailed in ref. [44], whereas the TiO_2/-biochar ratios in the impregnation process ranged between 0.1 and 1.5, as suggested for supporting TiO_2 on carbonaceous materials [51]. The calcination temperatures of the PP-TiO_2/biochar composites were taken from previous experimental runs conducted by the authors. It is worth mentioning that the calcination process sought to improve the dispersion of the TiO_2 particles in the biochar matrix, as suggested in ref. [52] and by some prior experimental findings of the authors. With a good dispersion of the semiconductor particles in the biochar, an improvement in the photocatalytic efficiency is expected. Besides, the TiO_2/-biochar load on the PP matrix was 1 % wt in all the films, which is within the range suggested for composite materials that use P25 TiO_2 [20].

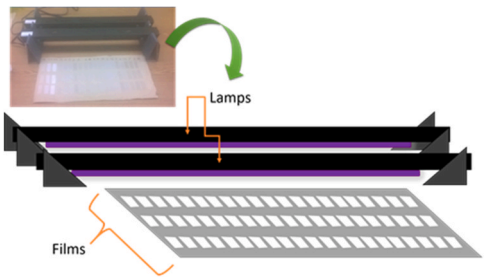

Fig. 1. Experimental setup for the photodegradation of the films.

Additionally, an analysis of variance (ANOVA) was performed to verify the model's suitability, together with the significance of the main factors and their interactions. The accuracy and applicability of the proposed model through the response surface methodology were evaluated through the statistical F value and the coefficient of determination (R^2 and adjusted R^2). The effect of photolysis (degradation of PP without TiO_2 or TiO_2/biochar) and the photodegradation of the films using TiO_2 alone (without biochar) was also evaluated. Therefore, photodegradation blanks were considered as shown in the experimental runs #18 –21 (Table 1). In addition, two replicates were made to evaluate the repeatability of the results. The optimization of the photodegradation of the films was carried out using Statgraphics 18.

3. Results and discussion

3.1. Plastic films production

Fig. S 1 portrays the images of the PP-TiO_2/biochar (or PP-TiO_2/biochar) pellets manufactured by the extrusion process and the commercial virgin PP pellets used in this work. The figure shows the blackish coloration of the pellets containing biochar, while those containing TiO_2 without biochar show a lighter shade, due to the presence of TiO_2. Additionally, Fig. 2 shows the films obtained by thermocompression.

Table 1
416B-type central-hybrid experimental design for evaluating the TiO_2/biochar synthesis conditions on the films photodegradation.

Experimental run	Pyrolysis temperature, °C	Oxygen content in pyrolysis, %	TiO_2/ biochar ratio	Calcination temperature, °C
1	350	2.50	0.80	800
2	350	2.50	0.80	246
3	304	0.85	0.34	488
4	396	0.85	0.34	488
5	304	4.15	0.34	488
6	396	4.15	0.34	488
7	304	0.85	1.26	488
8	396	0.85	1.26	488
9	304	4.15	1.26	488
10	396	4.15	1.26	488
11	420	2.50	0.80	30
12	280	2.50	0.80	30
13	350	5.00	0.80	30
14	350	0.00	0.80	30
15	350	2.50	1.50	30
16	350	2.50	0.10	30
17	350	2.50	0.80	321
18	Pristine PP			
19	PP-TiO_2–0.1wt%			
20	PP-TiO_2–0.5wt%			
21	PP-TiO_2–1.0 wt%			

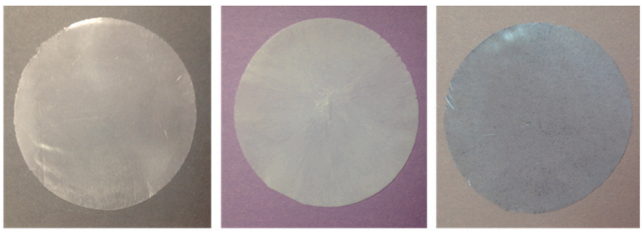

Fig. 2. Plastic films produced in this work. a) Films based on virgin polypropylene. b) PP-TiO_2 P-25 films. c) PP-TiO_2/biochar films.

The average thickness of the films was 0.1 mm, and they were produced with a diameter of approximately 12 cm. Fig. 2 shows a visible homogeneous distribution of the filler materials in the modified films. In addition, this figure shows the development of a white color in the PP-TiO_2 formulation and a blackish color in the PP-TiO_2/biochar formulation. These shades varied slightly with the composition of the materials. On the other hand, the virgin PP films maintained a translucent appearance.

3.1.1. X-ray fluorescence (XRF) analysis of the films

Table 2 reports the percentage of titanium in the PP, PP-TiO_2 and PP-TiO_2/biochar-based plastic films detected through the X-ray fluorescence technique. Through this technique it was possible to verify that the synthesis of the PP films modified with TiO_2 or TiO_2/biochar allowed the semiconductor fixation in the plastic material since the values of the titanium concentration in the virgin polypropylene films were null. Virgin PP should not exhibit TiO_2 or Ti even though the detection limit of the XRF instrument is 0.01 % (100 ppm). Nonetheless, lower Ti contents could be detected in other studies where TiO_2 was inserted in PVC, PP, and HDPE matrices [53]. The XRF analysis also reported Ti contents in polymer-derived ceramics pyrolyzed at different temperatures [54]. So, the XRF's capability and detection limit can guarantee that low values would not alter the analysis presented in the document.

The highest titanium concentration was found in PP/TiO_2 films (PP and TiO_2 only) at 1 % (1.0 wt% TiO_2 in the film). It is believed that this high TiO_2 content conferred this type of films a good photodegradation performance, as will be shown later in Section 3.2.1. Furthermore, in Table 2 can be observed that for samples prepared with low values of the TiO_2/Biochar ratio in the impregnation (Ti/Bc of 0.1 and 0.8), a relatively low titanium (TiO_2) fixation in the films is obtained, while when the ratio is high, in general, high values of titanium fixation were obtained. These results are generally congruent with the composition results of the TiO_2/Biochar samples detected by XPS (see Section 3.2.2 from ref. [37]). However, it is worth mentioning that the XRF results indicated that sample #1, despite having one of the lowest TiO_2/Biochar ratios (0.8), presented a relatively high percentage of titanium in the films. The reason could be the formation of Ti—O—C bonds generated in the calcination of the TiO_2/Biochar samples at 800°C, detected by X-ray emitted photoelectron spectroscopy (XPS) and infrared spectroscopy (FTIR-ATR) (See Sections 3.2.2 and 3.2.4 from ref. [37]). These bonds would allow TiO_2 particles to be fixed in high proportion in the biochar and in the plastic films after extrusion with PP.

In addition, the surface area of the TiO_2/biochar samples could also have been a determinant in the ultimate presence of titanium. As was shown in previous work [37] for example, when analyzing the surface area, [36]values of samples # 1 and 10, which have higher surface area values (171.2, 145.8 m^2/g), compared to samples #17 and 7, which have lower surface area values (40.6, 75.6 m^2/g); a higher percentage of titanium (0.7, 0.75 vs. 0.5, 0.5 percentage of Ti for films #1,10, 17 and 7 respectively) is observed in the films for the samples with higher surface area. Exceptional is the case of sample #15, for which the percentage of Ti in the films was 0.75 and the surface area of TiO_2/Biochar was 41.7 m^2/g. In this case, a possible explanation for the high value of titanium concentration in the films is the use of a high titanium/Biochar ratio in the impregnation tests (TiO_2/Biochar ratio = 1.5).

Table 2
Percentage of titanium in plastic films estimated by XRF.

Type of film*	Tpyrol, °C	% O_2	TiO_2/ Biochar	TCal, °C	% Ti
1	350	2.5	0.8	800	**0.7**
2	350	2.5	0.8	246	**0.8**
3	304	0.85	0.34	488	**0.45**
4	396	0.85	0.34	488	**0.4**
5	304	4.15	0.34	488	**0.4**
6	396	4.15	0.34	488	**0.45**
7	304	0.85	1.26	488	**0.5**
8	396	0.85	1.26	488	**0.8**
9	304	4.15	1.26	488	**0.625**
10	396	4.15	1.26	488	**0.75**
11	420	2.5	0.8	30	**0.55**
12	280	2.5	0.8	30	**0.6**
13	350	5	0.8	30	**0.6**
14	350	0	0.8	30	**0.55**
15	350	2.5	1.5	30	**0.75**
16	350	2.5	0.1	30	**0.1**
17	350	2.5	0.8	321	**0.5**
Pristine PP* *	-	-	-	-	**Undetectable**
PP-TiO_2 (1 %)	-	-	-	-	**1.53**

*Film type refers to the films that were produced with the materials corresponding to the experimental design shown in Table 1.
* *PP-virgin and PP-TiO_2 (1 %) correspond to films obtained with virgin polypropylene and extruded polypropylene with 1 % TiO_2, respectively.

3.2. Photodegradation of the plastic films

3.2.1. Weight loss results

The degradation of the pristine PP, PP-TiO_2 and PP-TiO_2/biochar based films, evaluated as the weight loss (see Eq. (1)), is presented in Table 3. This table indicates that the presence of TiO_2 or TiO_2/biochar particles cause weight loss of the polymer films during photoexposure, while the photoexposure of virgin PP films (films without TiO_2 or TiO_2/biochar) has a negligible effect on weight loss. These results agree with previous studies on the photodegradation of polyolefins with TiO_2 and other semiconductors [20,21,47], which reported that the semiconductor accelerates the polymer photodegradation process. In contrast, the exposure of the virgin polymer under similar radiation conditions causes slight changes in its mass. Table 3 shows that the percentage degradation of films containing only PP and TiO_2 increases with TiO_2 content, reaching a maximum degradation of 16.5 % with the formulation PP-TiO_2 - 1 % (polypropylene extruded with 1 % wt. TiO_2). The degradation of PP films with 0.5 % TiO_2 was ~5 times higher compared to films with a concentration of 0.1 % TiO_2; in turn, the degradation of films with 1 % TiO_2 was ~16 times higher than that obtained with 0.1 % TiO_2 and 3 times higher than that obtained with 0.5 % TiO_2. This behavior is because at higher concentrations of the photocatalyst, there is a more significant number of adsorption sites favoring the generation of oxidizing species that promote the degradation of the polymer.

Regarding the TiO_2/Biochar material, the highest degradation values were obtained with films # 2, 7, 9, 12 and 15, exhibiting degradations between 6.9 % and 8.7 %. Conversely, film type #15 (obtained with biochar synthesized at 350°C and with 2.5 % v/v in the pyrolysis reaction, with a TiO_2/biochar ratio of 1.5 in the impregnation process and without calcination) showed a degradation percentage of 8.7 %, which is equivalent to more than half of the maximum degradation (16.5 %). This result may be attributed to the relatively high concentration of TiO_2 that this type of film had (0.75 % of Ti content, according to the Table 2)

Table 3
Degradation of the plastic films with exposure time of 25 days under UV radiation (peak wavelength of 368 nm).

Type of film*	Tpyrol, °C	% O_2	TiO_2/ biochar	TCal, °C	Degradation (%)
1	350	2.5	0.8	800	1.7
2	350	2.5	0.8	246	6.9
3	304	0.85	0.34	488	1.3
4	396	0.85	0.34	488	1.3
5	304	4.15	0.34	488	1.5
6	396	4.15	0.34	488	1.8
7	304	0.85	1.26	488	7.4
8	396	0.85	1.26	488	5.2
9	304	4.15	1.26	488	7.7
10	396	4.15	1.26	488	6.1
11	420	2.5	0.8	30	4.4
12	280	2.5	0.8	30	7.9
13	350	5	0.8	30	6.5
14	350	0	0.8	30	5.9
15	350	2.5	1.5	30	8.7
16	350	2.5	0.1	30	0.2
17	350	2.5	0.8	321	5.3
18 (Pristine PP**)	-	-	-	-	0
19 (PP-TiO_2 - 0.1 %)	-	-	-	-	1.0
20 (PP-TiO_2 - 0.5 %)	-	-	-	-	5.4
21 (PP-TiO_2 - 1 %)	-	-	-	-	16.5

*Film type refers to the films produced with the materials corresponding to the experimental design shown in Table 1.
* *Pristine PP and PP-TiO2 (0.1, 0.5 and 1.0 %) correspond to films obtained with virgin polypropylene and polypropylene extruded with 0.1, 0.5, and 1.0 % TiO_2, respectively.

since the number of active sites promoting photodegradation is proportional to the catalyst concentration.

Fig. 3 shows the evolution of the degradation of various types of films during photoexposure. The figure displays a remarkable difference between the degradation obtained in films 21 and 15 (corresponding to those made with TiO_2 and TiO_2/biochar according to the conditions shown in Table 1) compared to films #18, which are those made of virgin PP. Even though PP and TiO_2 samples showed the highest degradation (~16 %), the PP-TiO_2/biochar formulation behaved similarly. These formulations are environmentally and economically beneficial because of the use of a material (biochar) extracted from biomass waste (coconut shells).

These results are similar to those obtained in previous works where a

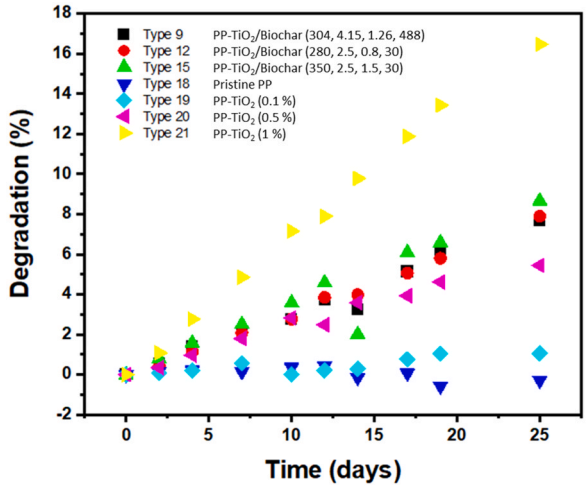

Fig. 3. Weight loss evolution of plastic films.

semiconductor was used as a photocatalyst. Bustos et al. reported a weight loss of ~1.35 % after 8.5 days of photoexposition for PP films modified with quasi-spherical zinc oxide nanoparticles (1.0 % wt.) [47]. Otherwise, Garcia-Montelongo et al. reported a ~8 % weight reduction of PP films modified with 1 % wt. TiO_2 P25 after six days of photoexposure [20]. Compared to the results shown in Fig. 3, the modification with the commercial P25 exhibited better photodegradation because the intrinsic properties of this material and the experimental conditions were different than those considered in this study (e.g. higher radiation intensity and a different brand of PP). Other studies have explored PP (or other polymers) photooxidation as an inconvenient feature [54–56], so the research target is to assure polymer stability. However, polymers' photodegradations were assessed in these previous reports, and they are much lower than the achieved ones with the TiO_2/biochar materials. This difference evidences the positive effect of the TiO_2/biochar modification for faster PP photodegradation.

3.2.2. *IR spectroscopy of the photodegradable films*

Fig. 4 shows the infrared transmittance spectra of three selected films on days 2, 19, and 25 of photoexposure with ultraviolet radiation. The figures show the spectra of virgin polypropylene (#18 of the experimental design in Tables 1), 1.0 % PP-TiO_2 (#21 of the experimental design in Table 1), and PP-TiO_2/biochar #15 of the experimental design in Table 1. The latter film was produced with biochar obtained at 350°C and 2.5 % O_2 in pyrolysis, with a TiO_2/biochar impregnation ratio of 1.5 and without the subsequent calcination step. Films 15 and 21 were selected since the highest weight loss was achieved on them (see Fig. 3), while virgin PP films were taken as reference. The presence of several signals associated with PP before and during photoexposure was verified using FTIR analysis. Among them, one can list the symmetric and asymmetric stretching of the CH_3 and CH_2 functional groups (methylenes and methylenes) comprised between 2840 and 2950 cm^{-1}, the deformation of methylenes and methylenes at 1460 and 1380 cm^{-1}, and a medium intensity signal associated with the stretching of the C—C bond, at ~1160 cm^{-1} [57,58]. Fig. 4 indicates that these signals appeared significantly during photoexposure tests on all types of films.

On the other hand, to verify that the insertion of TiO_2 and TiO_2/Biochar particles in the polymer matrix increased the photodegradation of the films, the evolution of carbonyl groups was monitored. These groups, which are detected around 1715 cm^{-1} in the infrared spectrum, appear in low molecular weight compounds that are generated during photooxidative reactions of polyolefins such as PE and PP [20,47,48]. Among the low molecular weight products generated are reported lactones, esters, ketones, carboxylic acids, etc. [20,47,48]. It is interesting to note that in Fig. 4b) and c), which describe the infrared spectra on days 19 and 25 of photoexposure, peaks appear around 1715 cm^{-1} for films #15 and 21, which correspond to the films containing TiO_2/-biochar and TiO_2. In contrast, for the case of the virgin PP films in those figures, the peak signal is negligible. On the other hand, Fig. 4a) does not show a significant signal around this peak for any of the films, which is reasonable because it corresponds to the early stages of photodegradation (day #2). The appearance of these peaks on days 19 and 25 of the tests may suggest that the presence of TiO_2 and TiO_2/Biochar initiated and/or accelerated the photooxidation of the polymer matrix, giving rise to lower molecular weight compounds containing carbonyl groups.

On the other hand, an increase in the signals of OH groups between 3050 and 3570 cm^{-1} is also detected in the films as photoexposition proceeds. An augmented view of Fig. 4, especially in the film #21 (compare spectra from day 0, 19, and 25) permit to have a better glimpse of the signals. As an example, Fig. S 2 shows the magnified OH absorbance peaks of the #15 and #21 samples. These signals appear due to the formation of hydroperoxide and alcohol type compounds during the photooxidation process [21,48] and also due to the moisture present in the films due to their hydrophilic capacity. The signal is detected with higher intensity for the PP-TiO_2 composite, given the high hydrophilic

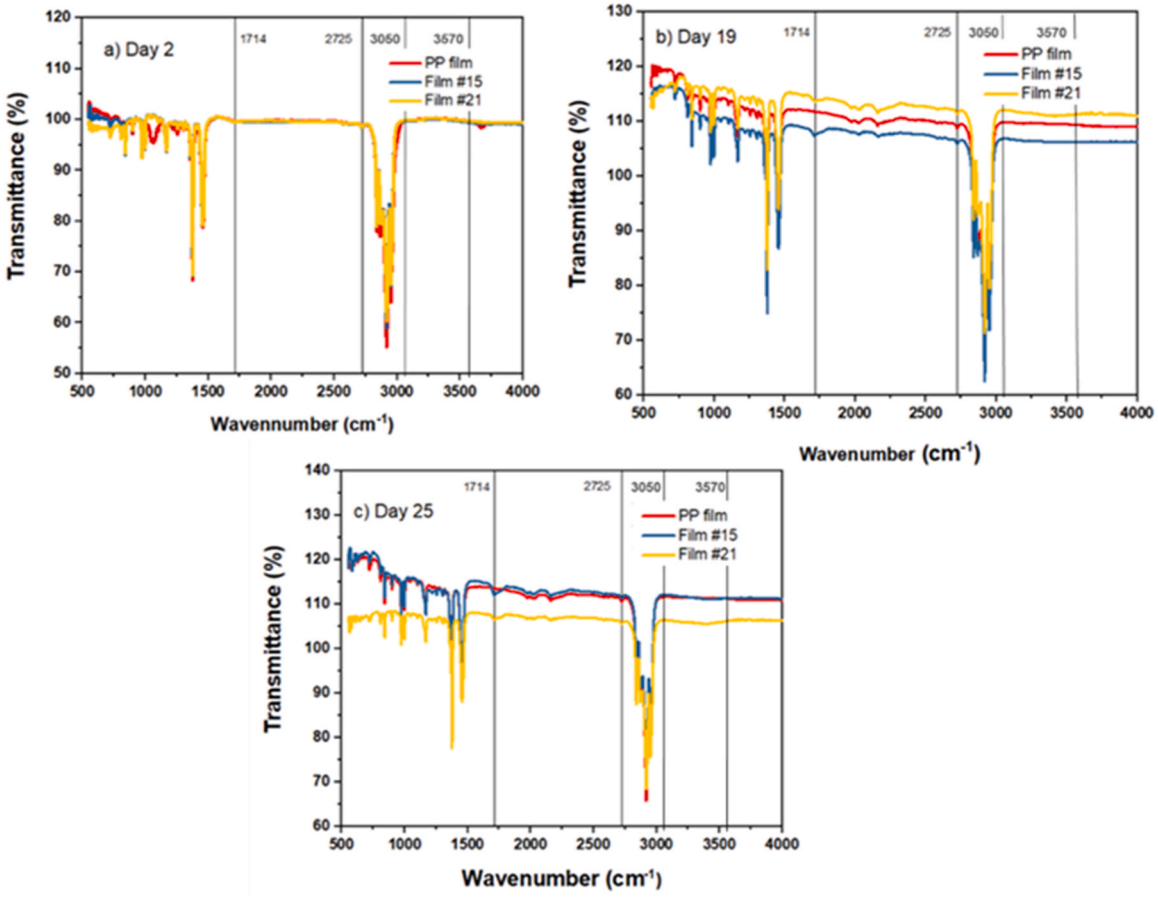

Fig. 4. Infrared spectrograms of the photodegradable films on days: a) 2, b) 19, and c) 25 of photoexposure. PP: indicates virgin polypropylene film, while #15 and #21 indicate the type of film according to the experimental design shown in Table 1.

capacity of TiO_2, in conjunction with the high photocatalytic activity that generates the oxidation products mentioned before.

The potential effect of the dipolar coupling on the measurements and characterization of the possible chemical compounds is determined by the size of these molecules [59]. This effect is stronger for the OH-based compounds than the CO-based ones. In our case, the oxidation by-products are mostly low-molecular compounds unaffected by a dipolar coupling.

Once these data were obtained, the carbonyl index was estimated (see Eq. (2)), which is one of the most used parameters for the evaluation of the extent of polypropylene degradation [20,47,48]. Table 4 reports the carbonyl indices of the samples after the end of the photoexposure process (day 25). As expected, the carbonyl and hydroxyl indices of the virgin PP films after the end of the photoexposure process were low (0.8 and 0.0, respectively), especially considering the duration of the degradation process (25 days). This finding is consistent with that reported in the literature for the photooxidative degradation of polypropylene [20,47,48]. Garcia-Montelongo et al. [20] and Bustos-Torres et al. [47] found carbonyl indices with values around ~2.6 and ~2.4 for the degradation of PP modified with TiO_2-P25 and ZnO, respectively; while for virgin PP, the carbonyl indices were 0.4 and 1.7, respectively. As for virgin PP, the results of these authors agree with those obtained in our work, which indeed indicates that the photooxidation of this unmodified polyolefin is reduced. On the other hand, our CI values for PP modified with TiO_2 and TiO_2/Biochar are higher than the cited works, which may be associated with the duration of the photodegradation process. However, recently, Prasert et al. [60] reported CIs of ~3.4 for PP specimens modified with up to 2w/w% of ZnO that were subjected to more than 18 weeks of exposure to sunlight (UV index in the experiments comprised between 8 and 14), which is a much longer time than that used in our work.

Generally, it is considered that the photooxidation of polypropylene is associated with the abstraction of its tertiary carbon hydrogens, by means of the attack of free radicals formed by the decomposition of impurities (carbonyl groups, peroxides, hydroperoxides and unsaturations) of the polymer that originate during its synthesis and processing [48,57,61,62]. Under weather conditions and absence of these initiating agents, the photodegradation of PP is very limited due to its low absorption of energy from the incoming solar spectrum at the earth's surface [48] and to the presence of stabilizers. On the other hand, it is reported that when the polymer is exposed to high-intensity radiant sources with emission wavelengths between 320 and 290 nm, photolysis of the polymer could proceed, since there would be a greater probability of breaking the C—C (energy bond of 375 kJ/mol, energetically equivalent to 320 nm radiation) and C—H (energy bond of 420 kJ/mol energetically equivalent to 290 nm radiation) bonds present in its structure [20]. In our work, photoexposure tests were carried out with UV radiation lamps with peak emission at 368 nm, with maximum irradiance value of 1.75 x 10^{-5} W/cm^2 nm for that wavelength. For this reason, low photodegradation values of the virgin polymer were observed, which agrees with the weight loss results reported in Fig. 3.

Table 4
Carbonyl and hydroxyl index of films in day 25 of photo-exposure.

Type of film	Carbonyl index	Hydroxyl index
Virgin PP	0.8	0.0
PP-TiO2/Biochar (#15)	11.4	10.5
PP-TiO2 (#21)	7.5	18.1

Now, the high carbonyl and hydroxyl indices for the samples with TiO_2 and TiO_2/biochar show that the incorporation of these materials into the polymer matrix could have accelerated their degradation process, as lower molecular weight compounds containing carbonyl and hydroxyl groups were formed [20,47,48]. The weight loss of the films reported in Fig. 3 suggests that the carbonyl and hydroxyl indices for these samples would be higher than those of the virgin PP films at the end of the photoexposure period, assuming a direct relationship between mass loss and the appearance of carbonyl indices. However, the results did not show a direct relationship, as Fig. 3 shows that the degradation was higher for the PP-TiO_2 (1 % wt) films, while the carbonyl index (Table 4) suggests that the generation of compounds with carbonyl groups was more important for the TiO_2/biochar films (#15 in the experimental design) compared to the PP films modified with TiO_2 alone (1 % wt).

On the other hand, the hydroxyl index for films with 1 % TiO_2 was higher than that of films with TiO_2/Biochar (#15), with values of 18.1 vs. 10.5, respectively. This result would be more in agreement with the photodegradation values evaluated with the weight loss shown in Fig. 3, in which, for the films with TiO_2 (1 % wt) a degradation of 16.5 % is shown, while for the TiO_2/Biochar (#15) films a degradation of 8.7 % was obtained. One explanation for the higher carbonyl index values for TiO_2/Biochar films compared to films containing only TiO_2 could be the possible interaction of oxidizing radicals generated in the polyolefin decomposition process with the biochar particles. It has been previously reported that the biochar surface can acquire oxygen-rich functional groups (C═O, OH) when in the presence of oxygen [63] in conjunction with ozone, oxidizing chemical species or at elevated temperatures [64–66]. For example, it has been shown that ozone can react with the unsaturated rings of biochar to generate carbonyl or carboxylic groups [65]. In our case, instead of ozone, oxidizing species are generated in the photocatalysis process (OH●, HOO● radicals [20]), as well as in the regular (non-catalytic) polyolefin photooxidation process (ROO●, RO● [20,48]), which probably could have oxidized the biochar surface, causing an increase in the signal of carbonyl groups in the infrared spectra. On the other hand, it is worth mentioning that the appearance of these oxygen-rich functional groups may cause an increase in the hydrophilic character of the material [64,65], which would favor the degradation process by photocatalysis. It is possible that surface oxidation occurs more easily in the types of biochar obtained at relatively low pyrolysis temperatures such as those used in this work (280–420°C) [63,65], since they have a higher amount of aromatic carbons with a lower degree of stabilization, as reported in ref. [65]. Regarding the hydroxyl indices, it is worth mentioning that the signal detected in the infrared between 3200 and 3600 cm^{-1} could encompass both the presence of OH groups associated with low molecular weight compounds resulting from the photooxidation of PP, as well as the presence of adsorbed moisture, especially considering the high hydrophilic capacity of TiO_2 particles [45]. On the other hand, biochar particles can also have hydrophilic sites, especially when the presence of hydrophilic functional groups is important on its surface. In any case, the retention of moisture in the vicinity of the semiconductor is important for the performance of the photocatalytic process since it is required for the generation of OH● radicals, which are highly determinant in the photodegradation by advanced oxidation processes.

3.2.3. Statistical analysis (Pareto chart)

The standardized Pareto diagram indicating the effect of the 4 factors evaluated in this work (temperature and percentage (% v/v) of oxygen in the pyrolysis reactor, the TiO_2/biochar ratio in the impregnation process and the calcination temperature) on the degradation of PP-TiO_2/Biochar films is shown in Fig. 5. The vertical blue line indicates the limit above which the factors are statistically significant at a 95 % confidence interval, and according to the figure, the TiO_2/Biochar ratio in the impregnation process and the calcination temperature are the statistically significant factors at this confidence interval. These two factors

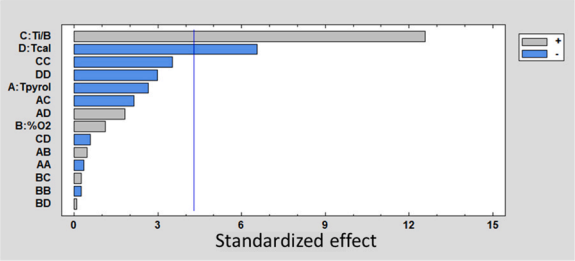

Fig. 5. Standardized Pareto diagram for the degradation of the PP-TiO_2/Biochar films. Factors: A: Pyrolysis temperature; B: % Oxygen in pyrolysis; C: TiO_2/Biochar ratio in impregnation; D: Calcination temperature.

have a greater effect on the degradation of the films than the pyrolysis temperature and the percentage of oxygen in the pyrolysis. Fig. 5 indicates that polymer degradation increases with increasing TiO_2/biochar ratio and decreases with calcination temperature. In turn, it shows that the increase in pyrolysis temperature causes a decrease in degradation, while the increase in oxygen content in pyrolysis increases it. Next, a deeper analysis of the effect of each factor on the polymer degradation is presented.

TiO_2/Biochar ratio

Increasing the TiO_2/biochar ratio increases the proportion of TiO_2 in the polypropylene films, which increases the rate at which oxidative species responsible for polymer degradation are generated. The XPS results [37] (Table S 2), indicate that as the TiO_2/biochar ratio increases, the elemental composition of titanium also increases in the TiO_2/biochar material; on the other hand, the XRF results reported in Table 2 show that the films fabricated with low values of the TiO_2/Biochar ratio in the impregnation presented a low percentage of titanium, while when the synthesis of the films was performed with high values of the TiO_2/biochar ratio, the percentage was higher. Since the percentage of TiO_2 in the films is proportional to the percentage of titanium detected in the films, then, in a general way, high values of the TiO_2/biochar ratio in the impregnation can be associated to higher concentrations of TiO_2 in the films. This would justify the results shown in the Pareto plot regarding the increase in degradation as the TiO_2/Biochar ratio in the films increases.

Contrariwise, as shown in Table S 1 (Fig. 5-c), the sample with the highest value of TiO_2/biochar ratio in the impregnation (TiO_2/biochar = 1.5) showed a shift of the signals in the XPS spectrum, possibly indicating a more significant interaction of the active sites of titanium dioxide with the biochar that could have influenced in the enhancement of the photocatalytic process. This shift in XPS-peaks positions (ascribed to the rise in the concentration of intervening species) has already been reported in the literature [67]. In our case, as mentioned before, it could be originated by the alteration of the chemical nature of the samples [68] by the higher interaction of TiO_2 with biochar particles [37].

Additionally, SEM images of TiO_2/biochar composites with high TiO_2/biochar ratio showed good distribution of TiO_2 on the biochar surface. For example, Table S 1 (Fig. 9-b) and Fig. S6 from ref. [37] show TiO_2/biochar particles with an impregnation ratio of 1.5 and 1.26, respectively, with good dispersion of TiO_2 in the biochar. The more homogeneous distribution of TiO_2 is favorable for the degradation the plastic films, as shown in other works where polyolefins are coupled with TiO_2 [32] and in Table 3 (see degradation of films #15 and 7, that correspond to the materials in Table S 1 (Fig. 9-b) and S6 from ref. [37], respectively). Additionally, the higher the proportion of TiO_2 particles in the films (due to a higher TiO_2/Biochar ratio in the impregnation process), the higher the number of centers with a highly hydrophilic character that would benefit the photocatalysis process. The results of the hydroxyl index presented in Table 4 could support this suggestion, considering that for the PP films modified with TiO_2 only the HI was higher than those modified with TiO_2/biochar. This could be associated

with the fact that TiO_2 particles have hydrophilic character [69], while biochar surface could have both hydrophilic and hydrophobic sites, depending on the functional groups present and the degree of carbonization of the material [64,70].

Lu et al. [71] report that the increase in the proportion of biochar in the TiO_2/biochar composite could cause a reduction in the photodegradation of contaminants, since the excess of biochar may block the passage of incoming radiation to the semiconductor. Then, with an increase in the TiO_2/biochar ratio in the impregnation process, one would have films with a lower proportion of biochar and thus less opportunity for blocking incoming radiation. A decreased radiation absorption could be a reason to explain the lower degradation values obtained for PP-TiO_2/biochar films compared to PP-TiO_2 films, as shown in Table 3 and Fig. 3. However, it would not correspond with the higher value of carbonyl index reported for PP-TiO_2/Biochar films (Table 4).

Calcination temperature

The calcination process sought to improve the dispersion of the TiO_2 particles in the biochar matrix as suggested in ref. [52] and the previous tests of this work. With a good dispersion of the semiconductor particles in the biochar, an improvement in the photocatalytic efficiency is expected. However, the images obtained through electron microscopy are not conclusive in this respect (See Table S 1 (Fig. 9a-b), and Figs. S 5 and S 6 from ref. [37]), since they show a similar distribution of TiO_2 particles in the biochar samples for different calcination temperatures (30, 488 and 800°C), with evidence of well-defined TiO_2 agglomerates in some areas (Table S 1 (Fig. 9-a) and S 5 from ref. [37]). On the other hand, the obtained surface area values (See Table 3 from ref. [37]) indicate that calcination increases the surface area of the material. For example, the surface area of the material with code[1] B-T 350, 2.5, 1.5, 30 is ~ 41.7 m^2/g, which is very similar to the surface area value of TiO_2 P25 (~ 50 m^2/g). This value is congruent, given that a TiO_2/Biochar weight-to-weight ratio of 1.5 was used to obtain this type of material (i.e., there was a higher proportion of TiO_2 P25 in the composite material) and there was no calcination. On the other hand, the specific surface area of the materials B-T 304, 0.85, 1.26, 488 and B-T 396, 4.14, 1.26, 488 are respectively ~ 75.6 and ~ 145.8 m^2/g. In this case, to obtain both materials, calcination at 488°C was performed with which an increase in surface area was obtained with respect to TiO_2 P25. It is also worth mentioning the behavior of material B-T 350, 2.5, 0.8, 800, which, despite having been synthesized with a low TiO_2/Biochar weight-weight ratio (0.8), presented a high surface area value (~ 171.2 m^2/g), caused by the high calcination temperature. The surface area is an important property in photocatalytic applications because it allows a better interaction between the contaminants and the catalyst, facilitating the adsorption and thus increasing the probability of attack of the radicals or photogenerated species to the molecules of interest [57,72].

Furthermore, the IR and XPS analysis of the TiO_2/biochar samples showed that at high calcination temperatures (800 °C) TiO_2 with biochar can interact via Ti−O−C bonds (See Table S 1 (Figs. 5 and 6)). This type of interaction could be the cause of the Eg (band gap energy) reduction (2.73/3.05 eV compared to 3.07 eV for TiO_2 P25, see Table 4 from ref. [37,73,74].

However, according to the Pareto diagram shown in Fig. 5, the effect of calcination temperature on degradation is negative, meaning that the higher the calcination temperature, the degradation of PP-TiO_2/Biochar films decreases. A possible explanation for this effect could be given by examining the crystallography of the material synthesized at different values of calcination temperature, as shown in Table S 1 (Fig. 4). The diffractogram in Table S 1 (Fig. 4c) from that reference shows that calcination at 800°C produced a change in the crystallinity of TiO_2 from anatase and rutile phases to another more unstable phase such as brookite, which is in agreement with the findings of other authors [75]. On the other hand, at calcination temperatures of 280 and 480 °C, the coexistence of the anatase and rutile phases is evident in Table S 1 (Fig. 4a-b), which is congruent with the composition of TiO_2 Degussa P-25 (80 % anatase, 20 % rutile). The existence of these phases directly affects the photocatalytic efficiency, since the anatase phase is more active than the rutile and brookite [75–77], which is associated with factors such as higher oxygen vacancies in the crystalline structure compared to brookite and rutile, anatase has a low dielectric constant and mass density, and high electron mobility [76]. Thus, according to this result, the increase in calcination temperature would decrease the photocatalytic activity and, this in turn, the degradation of the films [61]. Zhant al. [78] had similar findings regarding the effect of calcination temperature. They found that a low calcination temperature is suitable for better photocatalytic activity. Although these authors worked with TiO_2 precursors (tetrabutyl titanate and ethanol) to prepare TiO_2/biochar material, the calcination temperature produced less active TiO_2 phases [78].

Exploring the electrochemical characterization of the TiO_2/biochar materials is now advisable. The increase in calcination temperature causes an increase in the photocurrent generated by the illumination of these materials [37]. In the case of OCP (Fig. S 3 and ref. [37]), it was reported that for the material with higher calcination temperature (800°C), the potential showed a slower stabilization. This result agrees with the low photoluminescence intensities for the material calcined at 800°C (Fig. S 3 and ref. [37]). The higher photocurrent response, slower stabilization of the open circuit potential, and low photoluminescence may be indicators that at higher calcination temperature, TiO_2/biochar materials would have a lower recombination rate of the generated electron-hole pairs, which could be beneficial for the photocatalytic process, as it was reported in our previous work [37].

The crystallographic analysis of the materials (XRD) explains the electrochemical and photoluminescence responses found for the TiO_2/biochar materials calcined at elevated temperatures. For example, a well-defined signal at the position $2\theta = \sim 44$°C evidences the presence of the TiO_2/biochar material synthesized at a calcination temperature of 800°C [79] which is associated with carbon (Table S 1 (Fig. 4)),. In this case, the high calcination temperature may have contributed to the development of a more crystalline phase for the turbostratic layers of the biochar, which differentiated it from the broad signal (highly amorphous phase) presented for the same position in pure biochar as was shown earlier [44]). The higher the degree of turbostratic arrangement of the material, the greater the number of conjugations in the compound [70] that would improve the electrical conduction and the ability of the biochar to act as a sink for the electrons photogenerated in photocatalysis.

In this sense, there would be clear competition for the best photocatalytic response in terms of calcination temperature. On the one hand, with high calcination temperatures in the synthesis of TiO_2/biochar materials, a transition to TiO_2 phases with lower photocatalytic activity would occur, which would decrease the efficiency of the photocatalytic process. On the other hand, a higher calcination temperature would cause a higher degree of crystallinity in the carbonaceous phase which would contribute to a reduction in the recombination rate of the electron-hole pairs and therefore to a higher photocatalytic efficiency. Given this background, it is worth reconsidering the findings of IR and XPS spectroscopy. According to previous results [37], it was shown that the presence of hydrophilic groups such as C═O, C-O and COO on the biochar surface decreased with increasing calcination temperature, while the C−C (hydrophobic) groups increase. This result is congruent with that reported in the evolution of the chemical composition of biochars in thermal processes with low (or no) presence of atmospheric oxygen, where the progressive increase in temperature causes the loss of oxygen groups and concentrates carbon [70]. The increase in hydroxyl

[1] The B-T w,x,y,z code is taken from the experimental design. It indicates Biochar/TiO_2 obtained at w °C of pyrolysis temperature, x % of oxygen in pyrolysis, with a value of TiO_2/Biochar ratio in impregnation of y, and at z °C of calcination temperature.

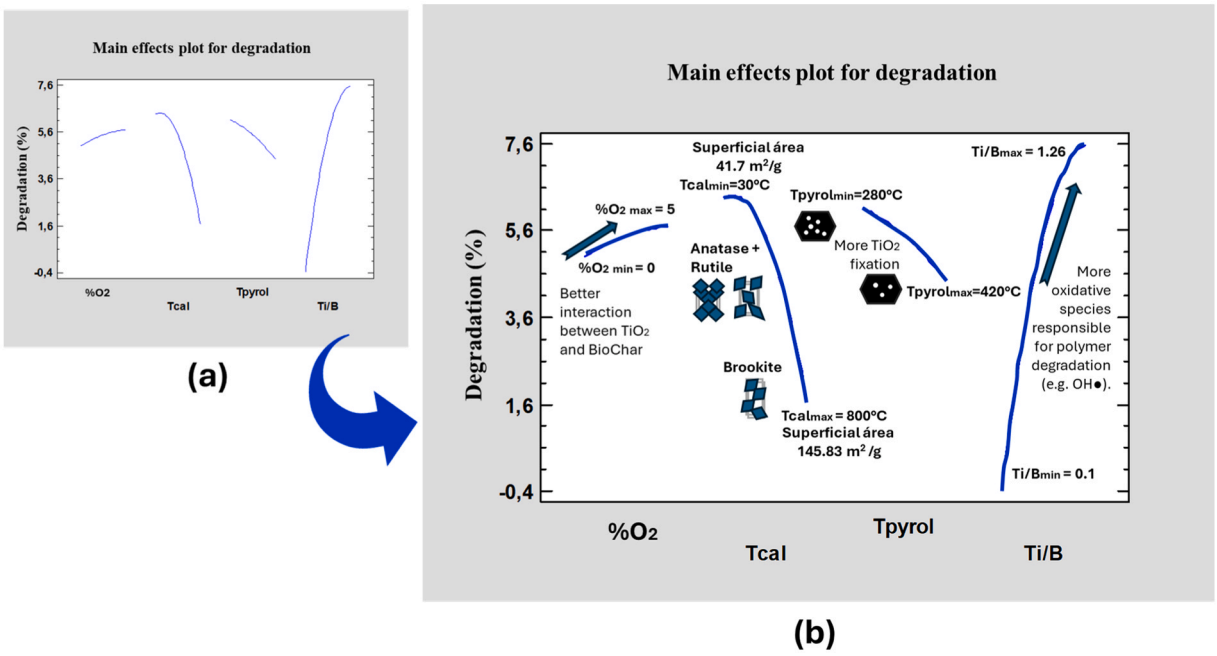

Fig. 6. Main Effect plot of the degradation percentage of the PP-TiO_2/biochar-based films. (a) Virgin plot. b) Same plot with the indication of changes of the material properties.

groups can give way to the increased capture of moisture in the vicinity of the material, which is important for the generation of highly oxidizing species such as hydroxyl radicals ($^{\bullet}OH$) that contribute highly to the destruction of organic pollutants by photocatalytic reaction. In that sense, it could be intuited that despite the advantages shown above for the use of elevated calcination temperatures for the TiO_2/Biochar material, the overall efficiency in the degradation of PP films synthesized with this material could be greatly reduced by the limitation in the interaction with the surrounding moisture.

Consistent with these results, Zhang et al. [78] reported that employing lower calcination temperatures when coupling TiO_2 with biochar would be more favorable because the biochar would lose to a lesser degree the original chemical and structural characteristics that can be beneficial to obtain better degradation of organic pollutants. The fact that the TiO_2/Biochar synthesis method uses low calcination temperatures (or no calcination), in addition to improving the overall efficiency in the degradation of PP-TiO_2/Biochar films as described in the previous paragraphs, could mean saving energy and economic resources for the future application of the technology.

Temperature and oxygen content in the pyrolysis reaction

According to the Pareto diagram, the effects of temperature and oxygen percentage in pyrolysis on film degradation are negative and positive, respectively. This means that the decrease in temperature and increase in oxygen percentage in pyrolysis tend to improve the degradation of plastic films.

One cause of this trend may be associated with the surface charge of the biochars. As was previously reported [37], when the pyrolysis temperature was increased, the Zeta potential of the biochar particles reaches values closer to the Zeta potential of the TiO_2 particles. This behavior could have caused the decrease of the interaction by electrostatic attraction [80] and attachment of TiO_2 particles on the carbonaceous materials and ultimately, reduce the photocatalytic efficiency as well. In contrast, as the percentage of oxygen in pyrolysis increased, the Zeta potential value of biochar particles moved further away from the Zeta potential value of TiO_2 particles. This could have led to better interaction by electrostatic attraction [70,80,81] and fixation of TiO_2 particles on the carbonaceous materials and ultimately also increase the photocatalytic efficiency. Wang and co-workers [70,81] used a similar approach to explain the better coupling of biochar particles with inorganic materials such as sand. The authors explained that as long as the biochar particles have Zeta potential values farther away from the sand particles, the total repulsive interaction energy will be lower, leading to better coupling between these materials [70,81]. Also, when surface charge of the particles is modified such as their difference increases (although their charge is still negative in both), the strong kinetic energy of the intervening particles may overcome the original energy barriers preventing the attachment of the particles [82]. The behavior can be extended to positive charges. On the other hand, when the difference of surface charge is reduced, the overcoming of these energy barriers is hindered, preventing the attachment between them, even with strong mixing conditions [82]. As a result, we expect that the larger difference in Zeta Potential between biochar and P25 TiO_2 particles observed in our work, promoted by the modification of the synthesis conditions of biochar, summed to the kinetic energy that they had during agitation/centrifugation, favored their interaction, as validated by the XPS, ATR, and SEM analyses previously reported. [37].

The XRF could support this suggestion. For the case of pyrolysis temperature, when comparing the titanium percentages in samples #11 and 12 reported in Table 2, in which all factors had equal values except for pyrolysis temperature. In this case, where the TiO_2/biochar materials were not subjected to calcination (30°C), a reduction in Ti concentration (and therefore TiO_2) is seen when going from a temperature of 280–420°C. The behavior may be different in other samples since other factors such as calcination temperature and TiO_2/Biochar ratio are involved. In the case of oxygen percentage, when comparing the titanium percentages in samples #13 and 14 reported in Table 2, an increase in Ti concentration (and therefore TiO_2) is evidenced when going from an oxygen percentage of 0–5 %.

Additionally, when the biochar was produced at 280°C, 350°C and 420°C, with oxygen percentage at 2.5 %, the surface area of the material initially increased with the pyrolysis temperature (~ 13.28 to ~ 15.57 m^2/g) and later decreased to ~ 9.85 m^2/g with the highest temperature (420°C) [44]. This behavior could also affect the ability of the biochar to retain TiO_2 particles, supporting the XRF results of films # 11 and 12, mentioned in the previous paragraph. The surface area reduction of biochar during pyrolysis at elevated temperatures may be

associated with recondensation effects of the released volatile compounds, pore plugging and shrinkage of the material occurring after reaching the softening point [83–85]. Then, according to the methodology of biochar production and impregnation of TiO_2 particles with biochar employed in the present work, it could be suggested that high pyrolysis temperature values in the range employed (above 396°C up to 420°C) would decrease the possibility of coupling between these materials by reducing the surface area and thus, reducing the efficiency in the photodegradation process.

Moreover, it is worthwhile to analyze the presence of functional groups of carbonaceous materials exposed to different temperatures and oxygen percentage in the pyrolysis reaction. For this purpose, we analyzed the results of infrared spectroscopy (ATR-FTIR) of the biochar samples reported in previous work[44]. For example, as the pyrolysis temperature increases, a decrease in the signals corresponding to the OH bond stretching vibrations (3200 and 3500 cm^{-1}) can be seen. For the case of the percentage of oxygen in pyrolysis, this signal presents a less pronounced decrease as the percentage of oxygen in the pyrolysis increases (especially, at the higher value of oxygen percentage, 5 % v/v), compared to the intensity of the signal when the pyrolysis temperature is increased. This bond may be associated with water molecules or hydroxyl groups [86,87], which are hydrophilic. Similarly, as the pyrolysis temperature increases, a decrease in the signal between 1740 and 1700 cm-1 occurs (see Fig. 1 from ref. [44]), which is associated with the stretching of the C═O bond. This bond corresponds mainly to carboxylic acids, traces of aldehydes, ketones, and esters [86], which are also hydrophilic. On the other hand, when the percentage of oxygen in the pyrolysis atmosphere is increased, this signal remains with practically a constant intensity (see Fig. 2 from ref. [44]). Likewise, with the variation of the pyrolysis temperature, the three bands between 885 and 750 cm^{-1}, which are associated with aromatic compounds [86,87] (of hydrophobic character), are noticeable. However, in the case of oxygen percentage variation, the intensity of these signals decreased, especially with the highest oxygen content in the pyrolysis atmosphere (5 % v/v).

The XPS data (elemental content and Gaussian deconvolution) of the biochar reported in Section 3.1.1. from ref. [37] show that the increase in pyrolysis temperature caused an increase and decrease in the concentration of elemental carbon and oxygen, respectively (see, for example, the percentage compositions of the biochar samples obtained with 2. 5 % O_2 at 280°C and 420°C reported in Table S 1 from ref. [37]); an increase in the signal associated with C−C bonds and a decrease in the presence of C−O and C═O bonds (Figs. 2a, 2b, 3a, and 3b from ref. [37]) on the surface of biochar particles. Oppositely, the increase in the oxygen content in pyrolysis caused a decrease and increase in the concentration of elemental carbon and oxygen, respectively (see, for example, the percentage compositions of biochar samples obtained at 350 °C with 0, 2.5 and 5 % O_2 reported in Table S 1 from ref. [37], a decrease in the signal associated with C-C bonds and an increase in the presence of C-O, C═O and COO bonds (Figs. 2c, 2d, 3c,and 3d from ref. [37]) on the surface of biochar particles. The decrease in the ratio of oxygen to elemental carbon (O/C ratio) and the increase in the C−C bond signal may indicate that the biochar surface becomes more hydrophobic [88,89] with increasing pyrolysis temperature, which is supported by the reduction of polar (hydrophilic) C−O and C═O bonds mentioned above. The decrease in the presence of hydrophilic groups and the increase or significant presence of hydrophobic groups in the biochars promoted by enhancing the pyrolysis temperature could limit their coupling with the TiO_2 particles -which have hydrophilic character-, so that the photocatalytic activity of the composite material was reduced. On the other hand, the lower number of hydrophilic groups could have reduced the ability of the TiO_2/Biochar material to capture surrounding moisture, and thus also reduced the photocatalytic efficiency. As mentioned above, moisture is necessary for the generation of hydroxyl radicals, which are highly responsible for degrading organic matter in photocatalytic processes. However, the increase in the O/C ratio and the decrease in the C−C signal that occur with increasing oxygen percentage in the pyrolysis atmosphere may indicate that the biochar surface became less hydrophobic [88,89], which ultimately was beneficial for plastic degradation by photocatalysis using the TiO_2/-biochar composite.

For a better glimpse of the relationship of each main factor with the degradation of the modified polymer, the Main Effect Plot is presented in Fig. 1(a). In this figure, both high and low-level values of each factor of the experimental design are shown. It can be observed that for low levels of oxygen percentage (0 %) and TiO_2/Biochar ratio (0.1) the degradation is low, around 0.6 % according to the statistical model, while for high levels of oxygen percentage (5 %) and TiO_2/Biochar ratio (1.5) a degradation of 11.5 % is obtained, possibly due to the increase in the generation of oxidative species (e.g. OH●) responsible for the plastic degradation, as stated earlier. For the other main factors, calcination temperature (Tcal) and pyrolysis temperature (Tpyrol), a different behavior is observed since the high levels of both effects (800°C and 420°C respectively) produced lower degradation (near to 2.8 %, according to the statistical model). It is because of a shift towards a less photoactive phase of TiO_2 (Brookite) (in case of the higher calcination temperature), and because of the possible reduction of the number of hydrophilic functional groups of the biochar (in case of the higher temperature of pyrolysis and calcination), in spite of the increase the superficial area increase from 41.7 m^2/g (Tcal=30°C) to 145.83 m^2/g (Tcal=800°C), also as stated earlier. In contrast, the low levels of Tcal y Tpyrol (30°C and 280°C respectively) lead to higher degradation (11.5 %) because they promote a higher impregnation of TiO_2 on the biochar surface and they are adequate to maintain the more reactive crystalline forms of titanium dioxide (Anatase and Rutile), as shown in Fig. 6(b).

It should be declared that since Tcal and the TiO_2/Biochar ratio are the most significant factors, a further new experimental design such as a block design [90] may be employed to mitigate the variability of the treatments and to understand more closely the incidence of both factors on polymer degradation. Nevertheless, in this work a surface response methodology was adopted for finding the numerical values of the factor levels that yield the maximum degradation. This strategy, shown in the next section, is statistically solid enough to optimize the response variable with confidence.

On the other hand, there could be concerns about the fact of using high amounts of energy in pyrolysis, in terms of transferring the contamination problem from the solid environment to atmosphere. This can be seen from two perspectives: one is the generation of gases that can be released to the atmosphere during pyrolysis, and the other is the generation of greenhouse gases resulting from the burning of fuels needed to reach the temperature required for the pyrolysis. One positive fact of the first one is that the generation of gaseous products from pyrolysis may be considered as a new source of energy or building block for obtaining new chemicals (i.e., syngas, [91,92]). With respect to the second one, there can be concerns about the possible amount of greenhouse gases that can be released into the atmosphere by burning (directly or indirectly) the fuel needed to perform pyrolysis. However, as progress in the use of renewable energy proceeds, there would be less need of burning fuels to support pyrolysis. BASF, for example, made a hint by employing electrically heated furnaces and not fuel-based to reach the high temperatures needed for generating pyrolysis products [93]. With this, huge amounts of greenhouse gases that affect the atmosphere are avoided to be released. In fact, the biochar used in our work was synthesized inside an electrically heated muffle receiving electricity which most of it ultimately came from the hydroelectric plants that nurture the city where the experiments were performed [94].

3.2.4. *Response surface methodology for film degradation*

The results of the experiments performed with the hybrid central experimental design 416B were used to obtain a mathematical model for the prediction of film degradation through the response surface methodology with Statgraphics 18. The mathematical model of film degra-

dation is presented below in Eq. (4), in which Tpyrol, $\%O_2$, $\frac{Ti}{B}$ and Tcalrepresent the pyrolysis temperature, oxygen content in pyrolysis, the ratio of TiO_2/biochar used in the impregnation process and the calcination temperature, respectively.

$$\begin{aligned}\%\textbf{Degradation} = & -2.43058 + 0.0166968 * \text{Tpyrol} - 0.354914 \\ & * \%O_2 + 20.5445 * \text{Ti/B} - 0.00899001 \\ & * \text{Tcal} - 0.0000386296 \\ & * \text{Tpyrol}^2 + 0.00148221 * \text{Tpyrol} \\ & * \%O_2 - 0.0242202 * \text{Tpyrol} \\ & * \text{Ti/B} + 0.0000338191 * \text{Tpyrol} \\ & * \text{Tcal} - 0.022261 * \%O_2^2 + 0.0823452 * \%O_2 \\ & * \text{Ti/B} + 0.0000522694 * \%O_2 * \text{Tcal} - 3.85568 \\ & * (\text{Ti/B})^2 - 0.0010934 * \text{Ti/B} \\ & * \text{Tcal} - 0.00000983988 * \text{Tcal}^2 \end{aligned} \quad (4)$$

Table 5 shows the ANOVA results for the quadratic model terms. This table also shows the values of the F-ratio and the P-value, indicating the most significant terms of the model. It should be recalled that the higher the value of the F-statistic and the lower the P-value, the more significant the term; and that P-values less than 0.05 indicate a significant regression at a 95 % confidence interval. The results agree with the Pareto diagram in Fig. 5, which indicates that the most significant factors are the ratio of TiO_2/Biochar in the impregnation and the calcination temperature. In addition, the R^2, adjusted R^2, standard error of the estimator, mean absolute error, and the root mean square error (RMES) are also reported.

The estimated R^2 and adjusted R^2 values show a good fitting of the quadratic model, which indicates the potential presence of optimum values for the response variable, whereas the standard error of the estimator, mean absolute error, and the RSME are also good indicators of the reliability of the proposed model.

The response surface plots are presented in Fig. 7, indicating the effect of the variables and their interactions on film degradation. However, considering a significance level of 0.05, the factors' interactions are insignificant. Despite these results, one can expect a significant interaction between some variables (e.g., calcination temperature and the TiO_2/biochar ratio). Nonetheless, the factors' levels considered in this study were crucial for the incidence of these factors and their interactions. Although the TiO_2 crystalline phase is strongly related to the calcination temperature, the photodegradation performance did not decrease or increase significantly with these factors' variations. The same consideration applies to a potential interaction between the pyrolysis temperature and the oxygen content.

Table 5
Analysis of variance (ANOVA) for the quadratic model of film degradation.

Source	Sum of Squares	DF	Mean Square	F-Ratio	P-Value
A:Tpyrol	3.23697	1	3.23697	7.11	0.1166
B:$\%O_2$	0.569513	1	0.569513	1.25	0.3798
C:Ti/B	72.0142	1	72.0142	158.1	0.0063
D:Tcal	19.5413	1	19.5413	42.9	0.0225
AA	0.0563448	1	0.0563448	0.12	0.7587
AB	0.10125	1	0.10125	0.22	0.6837
AC	2.10125	1	2.10125	4.61	0.1648
AD	1.48908	1	1.48908	3.27	0.2123
BB	0.0305525	1	0.0305525	0.07	0.8199
BC	0.03125	1	0.03125	0.07	0.8179
BD	0.0045515	1	0.0045515	0.01	0.9295
CC	5.61327	1	5.61327	12.32	0.0724
CD	0.155651	1	0.155651	0.34	0.618
DD	4.08114	1	4.08114	8.96	0.0958
Total error	0.911	2	0.4555		
Total (corr.)	125.729	16			

$R^2 = 99.2754$ %,
Adjusted $R^2 = 94.2034$ %
Standard error of the estimator = 0.674908
Mean absolute error = 0.103424
RMSE = 1.27265

So, Fig shows the response surface plots for film's degradation varying two factors. The values of the remaining factors were held constant at the midpoint. Additionally, Table 6 presents the combination of the levels of the experimental design factors that maximize the degradation of the PP-TiO_2/biochar films. This table presents that with low pyrolysis temperature (280°C), high oxygen percentage (~4.1 %), high TiO_2/Biochar ratio in the impregnation and low calcination temperatures (30°C) or no calcination, a maximum degradation value (11.5264 %) of the PP-TiO_2/Biochar plastic films could be obtained. The conditions that maximize the degradation of the films are obtained with the lowest energetic conditions in the thermal processes (low pyrolysis and calcination temperatures). This feature would undoubtedly represent an economic advantage for a potential commercial application of this technology. For example, assuming that calcination in a company producing the photodegradable PP-TiO_2/biochar films experiences a power consumption of 300 kWh for a daily operation (which has been reported for pyrolysis furnaces processing 10-ton batch of material, operating 10 h a day [95]), the annual savings associated to avoid calcination would be $ 8800 UDS (taking the energy cost as 8.04 cent/kWh [96]). In addition to this, the scaling of the plant producing the PP-TiO_2/biochar films will be less expensive since there would not exist the need of purchasing high-scale equipment for calcination. Now, in terms of running the pyrolysis at a lower temperature, as power consumption is proportional to the temperature increase experienced in the furnace, the energy and (costs) savings associated with the operation at a lower temperature would decrease accordingly [97,98].

Add, Table 6 shows that the optimum value of degradation was obtained with the highest TiO_2/biochar ratio (i.e., 1.5). This result means that the degradation maximizes when using the lowest value of biochar in the studied range of TiO_2/biochar mass ratio. As pointed out earlier, several authors have reported that the excess of biochar may block the passage of incoming radiation to the semiconductor [71], and thus reducing the benefits identified previously for biochar in biochar/TiO_2 systems, and for the PP degradation. This behavior may suggest exploring a wider range of TiO_2/biochar mass ratio in future works. Nevertheless, the fact that the TiO_2 nanoparticles are supported on biochar prevents the TiO_2 nanotoxicity. Consequently, the results from Fig. 3 for the PP-TiO_2/biochar composites are of significant relevancy for the photodegradation of PP, even if the results are not as high as those of the PP-TiO_2.

3.2.5. Proposed reaction mechanism for the photodegradation of PP-TiO_2/biochar compounds

The photodegradation of polymers has been previously studied in numerous papers [21,47,48,61]. In general terms, photodegradation is carried out by free radical attack reactions, which in case of PP are initially generated by the abstraction of hydrogen from the tertiary carbon of the repeating unit and in the presence of oxygen. Then, through successive reactions, more free radicals are generated which lead to the destruction of the polymer chains.

A well-accepted proposed mechanism for polymer degradation initiates with the formation of polymeric alkyl radicals (P●) through heat or radiation [47,48,61]. It is worth mentioning that in the presence of radiation and oxygen, the polymer degradation phenomenon is known as photo-oxidation [62]. The alkyl radicals then react with oxygen to form peroxyl radicals (POO●), which in turn can react with other macromolecules of the polymer, abstracting hydrogens from them and generating hydroperoxides (POOH) [47,48,61]. This series of steps is shown in Eqs. (5)-(8). Additionally, through radiation or heat, dissociation of the hydroperoxides can take place by cleavage of the O–O bonds [62] to generate alkoxy radicals (PO●), which in turn can be

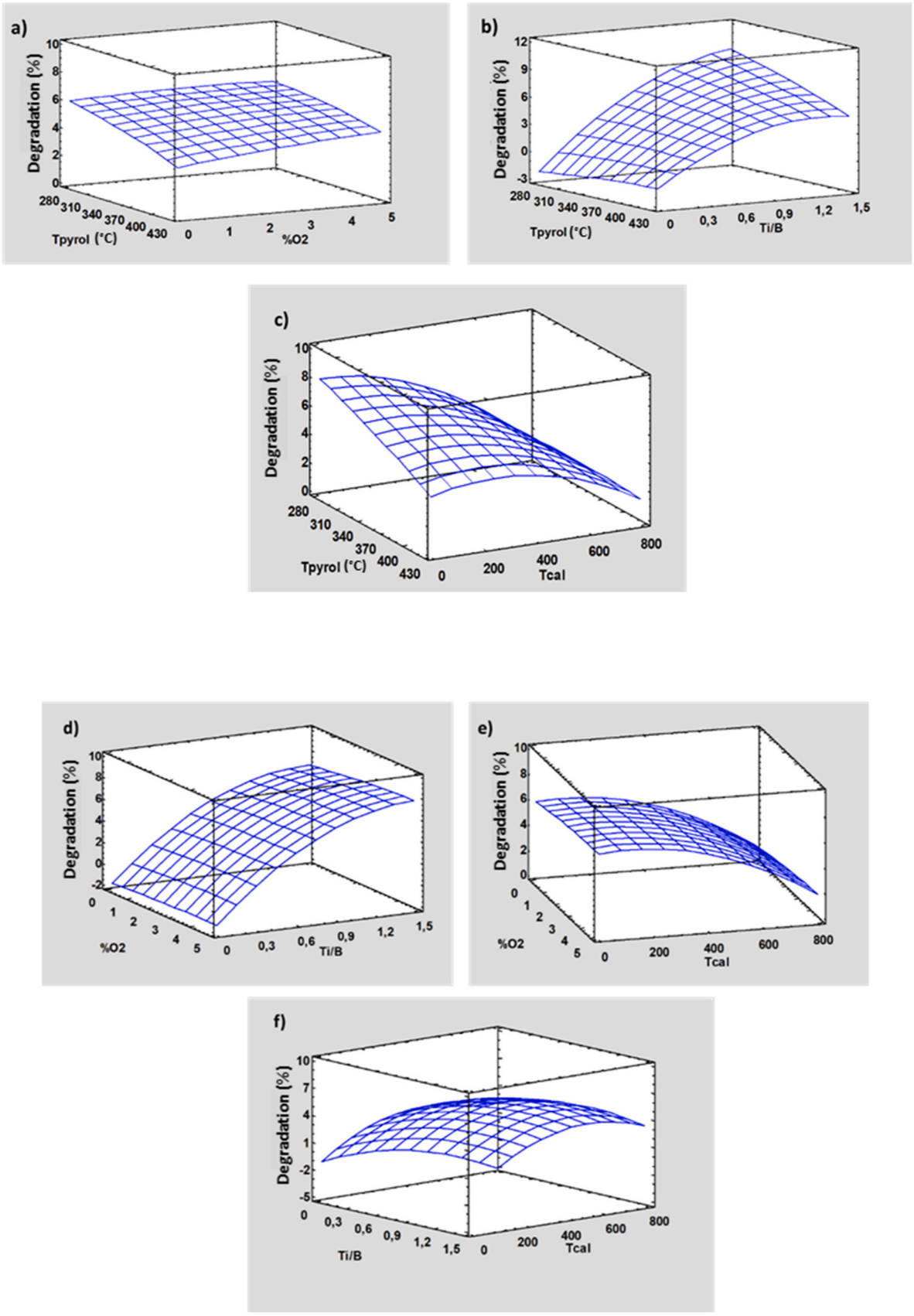

Fig. 7. Response surface plots for the factors analyzed in the hybrid design used for the photodegradation of the PP-TiO_2/Biochar films.

Table 6
Levels of experimental design factors that maximize the degradation of PP/TiO_2-Biochar films.

Optimum degradation value: 11.53 %			
Factor	**Low**	**High**	**Optimum degradation = 11.53 % at**
Pyrolysis temperatura	280.0 °C	420.0°C	280.0°C
Oxygen percentage in pyrolysis	0.00 %	5.00 %	4.09 %
TiO_2/Biochar ratio in impregnation	0.1	1.5	1.5
Calcination temperature	30.0 °C	800.0°C	~30.00 °C

decomposed by beta scissions into molecules of lower molecular weight, which may contain carbonyl groups [47,48,62] (see Eq. (9)). This series of steps then leads to the degradation of the polymer, which finally proceeds to the mineralization of the organic matter, i.e. the formation of CO_2 and water, as shown in Eq. (10) [20,57,62]. Within the lower molecular weight molecules generated in the beta-scission reactions of the PP photoxidation mechanism are reported: short chain alkanes such as methane, ethane, propane, butane and pentane; certain alkenes such as ethylene, propylene, 2-butene, among others; ketones such as propanone, hydroxy acetone and butanone; acetic acid, among others [57].

$$PH + O_2 \xrightarrow{\Delta,\ h\upsilon} P\bullet + OOH\bullet \quad (5)$$

$$P\bullet + O_2 \longrightarrow POO\bullet \quad (6)$$

$$POO\bullet + PH \longrightarrow POOH + P\bullet \quad (7)$$

$$POOH \longrightarrow PO\bullet + OH\bullet \quad (8)$$

$$PO\bullet \xrightarrow{\beta scission} C=O \text{ compouds and volatile compounds} \quad (9)$$

$$C=O \text{ compounds} \xrightarrow{h\upsilon} CO_2 + H_2O \quad (10)$$

Now, the presence of a semiconductor inside the polymer matrix can accelerate the photooxidation of the material since, by absorbing electromagnetic radiation with appropriate wavelength, the semiconductor can generate active species (mainly OH●, OOH●) that also lead to photo-oxidative degradation of the polymer through reaction with oxygen and water [61].

In the case of TiO_2, activation with radiation with energy above its band gap results in the formation of the well-known electron-hole pair (Eq. (11)). Photogenerated holes can react with surrounding water molecules (moisture, see Eq. (12)) or hydroxyl ions to generate hydroxyl radicals (OH●) [21,32,47], which are highly responsible for the degradation of organic matter. Similarly, photogenerated electrons can react with surrounding oxygen to form superoxide ions (Eq. (13)), which through subsequent reactions can give way to the generation of more oxidizing radicals (see Eqs. (14)-(17)) [21,32,47].

$$TiO_2 \xrightarrow{h\nu} e^-_{BC} + h^+_{BV} \quad (11)$$

$$H_2O_{ads} + h^+{}_{BV} \longrightarrow OH\bullet + H^+ \quad (12)$$

$$e^-_{BC} + O_2 \longrightarrow O_2^{\bullet -} \quad (13)$$

$$O_2^{\bullet -} + H_2O \longrightarrow HO_2\bullet + OH^- \quad (14)$$

$$2\ \ HO_2\bullet \longrightarrow H_2O_2 + O_2 \quad (15)$$

$$H_2O_2 \xrightarrow{h\upsilon} 2OH\bullet \quad (16)$$

$$OH^- + h^+{}_{BV} \longrightarrow OH\bullet \quad (17)$$

The hydroxyl radicals (OH●) generated through the photocatalytic mechanism can interact with the polymer molecules to also generate P● radicals, as shown in Eq. (18) [20,32], and thus, accelerate the photo-oxidation process previously described through Eqs. (5)-(9). Also, hydroxyl radicals can intervene in the mineralization of the lower molecular weight compounds generated in the oxidative process, as shown in Eq. (19) [20,47].

$$PH + OH\bullet \longrightarrow P\bullet + H_2O \quad (18)$$

$$C=O \text{ compounds} + OH\bullet \longrightarrow CO_2 + H_2O \quad (19)$$

Similarly, the photogenerated holes can react with the polymer to also produce P● radicals, as described in Eq. (20) [21,57], accelerating the oxidative process of the polymer.

$$PH + h^+{}_{BV} \quad + O_2 \longrightarrow P\bullet + HO_2\bullet \quad (20)$$

In the above equations, the photo-oxidative reaction mechanism that takes place in the degradation of polypropylene in the presence of TiO_2 alone is described. However, in the present work, the coupling of biochar with TiO_2 in polymer degradation was explored. It has been reported that the use of biochar in photocatalysis is beneficial because biochar acts as a sink for the electrons photogenerated in the photocatalytic reaction (Eq. (11)), so that it reduces the recombination of the hole-electron pair [100,155,164,189] and thus improves the efficiency in the pollutant degradation process. Open-circuit potential and photoluminescence analyses of this same type of TiO_2/biochar compounds effectively indicated that the presence of biochar reduces the rate of electron-hole pair recombination in the photocatalytic system [30]. It is worth remembering that electron-hole pair recombination reduces the generation of the highly oxidizing species in the photocatalytic process (e.g., Eqs. (12) and (17)) that are primarily responsible for the degradation of organic matter.

On the other hand, it has been reported that biochar can be oxidized in the presence of oxygen in conjunction with high temperature conditions or by chemical oxidizing agents to generate functional groups (C═O, OH, etc) on the surface of the material [63–66]. For example, ozone can react with the unsaturated rings of biochar to generate carbonyl or carboxylic groups on the material.

In this work, given the high probability of the generation of strong oxidizing species by photocatalysis and given that the polymer degradation takes place in the presence of oxygen, we propose that the photocatalytically generated OH● and HOO● radicals can oxidize the biochar so that carbonyl groups are generated on its surface. This would be in agreement with the mass loss and the carbonyl and hydroxyl indices of the photodegradable films reported in Table 3 and Table 4, where it is evident that the PP-TiO_2/Biochar based films showed a higher value of the carbonyl index compared to the films synthesized with PP-TiO_2 alone, while the mass loss was higher for the latter. Accordingly, it could then be inferred that biochar is susceptible to oxidation leading to the formation of compounds containing carbonyl groups [63–65]. Then, in the case of the degradation of PP-TiO_2/Biochar films, the following stages would appear in the reaction mechanism, which would compete for the use of the oxidizing OH● and HOO● species:

$$Biochar + OH\bullet \longrightarrow C=O compounds \quad (21)$$

$$Biochar + HO_2\bullet \longrightarrow C=O compounds \quad (22)$$

The mechanism of polyolefin degradation through the action of photocatalysis (and in the absence of photocatalyst) with biochar-modified TiO_2, according to the previous discussion is illustrated in Fig. 8. The proposed reaction mechanism is valid at the different conditions of TiO_2/biochar ratio and temperature of calcination of the TiO_2/biochar explored in this work. As discussed earlier, the higher TiO_2/biochar ratio is expected to favor the appearance of the chemical species responsible for photooxidation of the polymer. This is because the

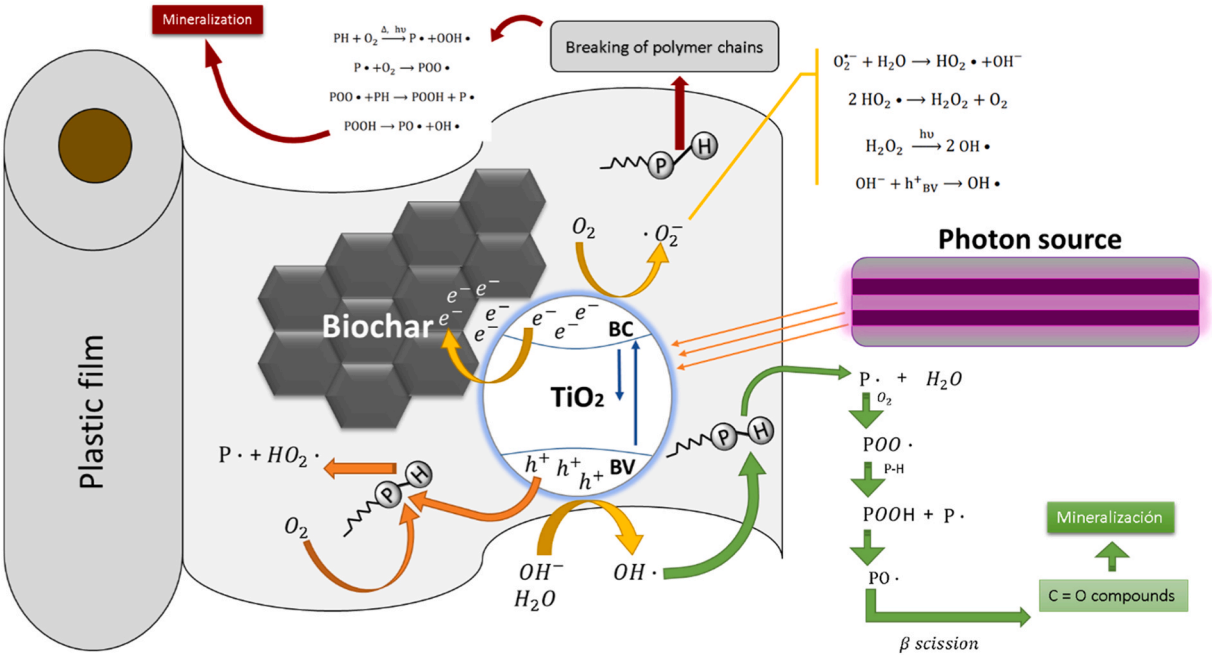

Fig. 8. Proposed mechanism for the photocatalytic degradation of PP with TiO_2/Biochar.

higher TiO_2 presence in the films, the higher active sites capable of generating the electron-hole pairs, and the higher hydrophilic nature (and moisture capture capability) of the TiO_2/biochar compound, both of which promote the OH● formation. However, it should be recalled that high calcination temperatures cause transition to less active phases of the catalysts, despite the band-gap reduction.

4. Conclusion

The application of photocatalysis with TiO_2 coupled with biochars derived from coconut shells and artificial ultraviolet radiation significantly accelerated the solid-phase degradation of polypropylene plastic films compared to virgin films. Extrusion and thermocompression techniques were used to synthesize PP plastic films and XRF analysis verified the effective incorporation of the semiconductor into the films. Even though the degradation of PP-TiO_2 films (1 % w/w) was higher than that observed for PP-TiO_2/biochar films, the weight loss and carbonyl index values obtained for the PP-TiO_2/biochar films were higher than those reported for PP films synthesized with other semiconductors. In addition, an analysis of the carbonyl index and the weight loss of the PP-TiO_2/biochar films suggests that the biochar surface oxidizes, giving rise to hydrophilic functional groups and increasing photocatalytic efficiency as reaction time proceeds. Besides, incorporating the TiO_2/biochar composite into plastic matrices would not cause a nanotoxicity threat as the TiO_2 nanoparticles are anchored in the micrometric biochars. According to the statistical analysis, the factors that most affect the degradation of PP-TiO_2/biochar films are the TiO_2/biochar mass ratio in the impregnation process and the calcination temperature in the synthesis of the TiO_2/biochar composite. A high TiO_2/biochar ratio in the impregnation process is positive because it allows a higher concentration of TiO_2 in the films and, therefore, a higher probability of generating oxidative species responsible for the degradation of organic matter by photocatalysis. Similarly, the high concentration of TiO_2 favors the increase of hydrophilic sites in the TiO_2/biochar material, which could improve both the capture of the surrounding moisture and the utilization of the incoming radiation, and therefore, also increase the generation of the highly oxidative species of photocatalysis.

On the other hand, high calcination temperatures, although decreasing the band gap of the catalyst and reducing the recombination of the hollow electron pair in the photoexposure of the material, cause a shift towards other phases of TiO_2 with different photoactivities than Aeroxide P25 and reduce the number of hydrophilic functional groups of the biochar, which in sum slows down the photodegradation of the films. Then, it is interesting from the point of view of photocatalytic efficiency and energy (and economic) savings to use low calcination temperatures for the fabrication of PP-TiO_2/Biochar films. The analysis of the TiO_2/biochar morphology revealed that with a high TiO_2/biochar ratio and low calcination temperature (30°C), a homogeneous distribution of TiO_2 in the biochar particles can be achieved, which is favorable for the degradation of the films. Conversely, the pyrolysis reaction favored PP degradation with low temperatures and high oxygen percentages (total range of 0–5 % v/v). With these conditions, there would be a better coupling between TiO_2 and biochar particles and a higher presence of hydrophilic groups (C═O, C−O) that would increase the photocatalytic efficiency, as indicated by Zeta potential, XPS, and FTIR analysis of the TiO_2 and biochar particles and XRF on PP-TiO_2/biochar films. This work shows an attractive and almost unknown alternative for coping with plastic pollution, which is believed to be very opportune nowadays when an even higher generation of plastic waste is seen.

CRediT authorship contribution statement

Castilla Caballero Deyler Rafael: Writing – original draft, Visualization, Validation, Methodology, Investigation, Data curation, Conceptualization. **Medina-Guerrero Astrid:** Writing – original draft, Methodology. **Barraza-Burgos Juan Manuel:** Supervision, Resources, Methodology, Conceptualization. **Roa-Espinosa Aicardo:** Supervision, Resources. **Gunasekaran Sundaram:** Supervision, Resources, Formal analysis. **Hernandez-Ramirez Aracely:** Writing – review & editing, Supervision, Resources, Methodology. **Vazquez-Rodriguez Sofia:** Supervision, Resources, Investigation. **Colina-Márquez José:** Supervision, Formal analysis. **Machuca Martínez Fiderman:** Supervision, Resources, Funding acquisition, Formal analysis.

Declaration of Competing Interest

The authors declare the following financial interests/personal

relationships which may be considered as potential competing interests: Deyler Rafael Castilla-Caballero reports financial support was provided by Minciencias (PhD studies and PhD internship) and Fulbright Colombia (PhD Internship). Fiderman Machuca-Martinez reports a relationship with Colombia Ministry of Science Technology and Innovation that includes: funding grants. Deyler Castilla-Caballero, Fiderman Machuca-Martínez, José Colina-Márquez, Juan Barraza-Burgos has patent "Películas fotodegradables de polipropileno que incorporan dióxido de titanio acoplado con biochars y su método de obtención" pending to Universidad del Valle and Universidad de Cartagena. Castilla-Caballero and Medina-Guerrero report marital relationship. None

Acknowledgements

Deyler Castilla-Caballero, José A. Colina-Márquez, Fiderman Machuca-Martínez, and Astrid Medina-Guerrero thank Colciencias (MinCiencias) for supporting their Ph.D. studies. Also, Deyler Castilla-Caballero gives special thanks to Fulbright-Colombia, the Universidad del Valle (CIAM grant) and Colciencias (MinCiencias) for funding his PhD internships. Assistance provided by the members of Prof. Gunasekaran's laboratory (especially Omer Sadak) and Rob McClain at the UW-Madison, and from the Wisconsin Institute for Discovery (especially Galip Yilmaz), is much appreciated. Colina-Márquez thanks to the Universidad de Cartagena via Grant No. 005–2023 which enabled him to contribute to writing this work. Finally, Castilla-Caballero and Medina-Guerrero acknowledge El Shaddai for His support during the research.

Data availability

The data is included in the manuscript

References

[1] S. King, K.E.S. Locock, A circular economy framework for plastics: a semi-systematic review, J. Clean. Prod. 364 (2022) 132503, https://doi.org/10.1016/J.JCLEPRO.2022.132503.
[2] N.N. Phuong, A. Zalouk-Vergnoux, L. Poirier, A. Kamari, A. Châtel, C. Mouneyrac, F. Lagarde, Is there any consistency between the microplastics found in the field and those used in laboratory experiments? Environ. Pollut. 211 (2016) 111–123, https://doi.org/10.1016/j.envpol.2015.12.035.
[3] D. Jubinville, E. Esmizadeh, S. Saikrishnan, C. Tzoganakis, T. Mekonnen, A comprehensive review on global production and recycling methods of polyolefin (PO) based products and their post-recycling applications, Sustain. Mater. Technol. 25 (2020) e00188, https://doi.org/10.1016/j.susmat.2020.e00188.
[4] Z. Fu, J. Wang, Current practices and future perspectives of microplastic pollution in freshwater ecosystems in China, Sci. Total Environ. 691 (2019) 697–712, https://doi.org/10.1016/j.scitotenv.2019.07.167.
[5] R. Thompson, C. Moore, F. vom Saal, S. Swan, Plastics, the environment and human health: current consensus and future trends, Phylosophical Trans. R. Soc. B 364 (2009) 2153–2166.
[6] Global plastic production 1950-2020 | Statista, (n.d.). ⟨https://www.statista.com/statistics/282732/global-production-of-plastics-since-1950/⟩ (accessed July 14, 2022).
[7] O.O. Fadare, E.D. Okoffo, Covid-19 face masks: a potential source of microplastic fibers in the environment, Sci. Total Environ. 737 (2020) 140279, https://doi.org/10.1016/j.scitotenv.2020.140279.
[8] E.M. Foundation, N. Plast. EcoN.: Rethink. Future Plast. (2016).
[9] A. Tullo, The cost of plastic packaging, Chem. Eng. N. 94 (2016) 32–37.
[10] R. Porta, The plastics sunset and the bio-plastics sunrise, 2019, Vol. 9, Page 526, Coatings 9 (2019) 526, https://doi.org/10.3390/COATINGS9080526.
[11] Ministerio de Ambiente y Desarrollo Sostenible, Resolución No. 0668 del 28 de abril de 2016, por la cual se reglamenta el uso racional de bolsas plásticas y se adoptan otras disposiciones, Colombia, 2016.
[12] C.M. Free, O.P. Jensen, S.A. Mason, M. Eriksen, N.J. Wiliamson, B. Boldgiv, High-levels of microplastic pollution in a large, remote, mountain lake, Mar. Pollut. Bull. 85 (2014) 156–163.
[13] E.E.P. Inc., TDPA®: Aditivo plástico totalmente degradable, (2016). ⟨http://www.epi-global.com/es/about-tdpa.php⟩.
[14] H. Du, S. Huang, J. Wang, Environmental risks of polymer materials from disposable face masks linked to the COVID-19 pandemic, Sci. Total Environ. 815 (2022) 152980, https://doi.org/10.1016/J.SCITOTENV.2022.152980.
[15] I.A. Hassan, A. Younis, M.A. Al Ghamdi, M. Almazroui, J.M. Basahi, M.M. El-Sheekh, E.K. Abouelkhair, N.S. Haiba, M.S. Alhussaini, D. Hajjar, M.M. Abdel Wahab, D.M. El Maghraby, Contamination of the marine environment in Egypt and Saudi Arabia with personal protective equipment during COVID-19 pandemic: a short focus, Sci. Total Environ. 810 (2022) 152046, https://doi.org/10.1016/J.SCITOTENV.2021.152046.
[16] K.P. Roberts, S.C. Phang, J.B. Williams, D.J. Hutchinson, S.E. Kolstoe, J. Bie, I.D. Williams, A.M. Stringfellow, Increased personal protective equipment litter as a result of COVID-19 measures, (n.d.). https://doi.org/10.1038/s41893-021-00824-1.
[17] R. Arriagada, F. Lagos, M. Jaime, C. Salazar, Exploring consistency between stated and revealed preferences for the plastic bag ban policy in Chile, Waste Manag. 139 (2022) 381–392, https://doi.org/10.1016/J.WASMAN.2021.12.040.
[18] P. Behuria, Ban the (plastic) bag? Explaining variation in the implementation of plastic bag bans in Rwanda, Kenya and Uganda:, ⟨Https://Doi.Org/10.1177/2399654421994836⟩ 39 (2021) 1791–1808. https://doi.org/10.1177/2399654421994836.
[19] M. Amenábar Cristi, C. Holzapfel, M. Nehls, D. De Veer, C. Gonzalez, G. Holtmann, D. Honorato-Zimmer, T. Kiessling, A.L. Muñoz, S.N. Reyes, P. Nuñez, J. M. Sepulveda, N. Vásquez, M. Thiel, The rise and demise of plastic shopping bags in Chile – Broad and informal coalition supporting ban as a first step to reduce single-use plastics, Ocean Coast Manag 187 (2020), https://doi.org/10.1016/j.ocecoaman.2019.105079.
[20] X.L. García-Montelongo, A. Martínez-De La Cruz, S. Vázquez-Rodríguez, L. M. Torres-Martínez, Photo-oxidative degradation of TiO2/polypropylene films, Mater. Res Bull. 51 (2014) 56–62, https://doi.org/10.1016/j.materresbull.2013.11.040.
[21] S.S. Ali, I.A. Qazi, M. Arshad, Z. Khan, T.C. Voice, Ch.T. Mehmood, Photocatalytic degradation of low density polyethylene (LDPE) films using titania nanotubes, Environ. Nanotechnol. Monit. Manag 5 (2016) 44–53, https://doi.org/10.1016/j.enmm.2016.01.001.
[22] R. Verma, S. Singh, M.K. Dalai, M. Saravanan, V.V. Agrawal, A.K. Srivastava, Photocatalytic degradation of polypropylene film using TiO2-based nanomaterials under solar irradiation, Mater. Des. 133 (2017) 10–18, https://doi.org/10.1016/j.matdes.2017.07.042.
[23] S. De Gisi, G. Gadaleta, G. Gorrasi, F.P. La Mantia, M. Notarnicola, A. Sorrentino, The role of (bio)degradability on the management of petrochemical and bio-based plastic waste, J. Environ. Manag. 310 (2022) 114769, https://doi.org/10.1016/J.JENVMAN.2022.114769.
[24] L. do Val Siqueira, C.I.L.F. Arias, B.C. Maniglia, C.C. Tadini, Starch-based biodegradable plastics: methods of production, challenges and future perspectives, Curr. Opin. Food Sci. 38 (2021) 122–130, https://doi.org/10.1016/J.COFS.2020.10.020.
[25] M.I. Din, T. Ghaffar, J. Najeeb, Z. Hussain, R. Khalid, H. Zahid, Potential perspectives of biodegradable plastics for food packaging application-review of properties and recent developments 37 (2020) 665–680, https://doi.org/10.1080/19440049.2020.1718219. ⟨Https://Doi.Org/10.1080/19440049.2020.1718219⟩.
[26] M. Motamedi, L. Yerushalmi, F. Haghighat, Z. Chen, Recent developments in photocatalysis of industrial effluents : a review and example of phenolic compounds degradation, Chemosphere 296 (2022) 133688, https://doi.org/10.1016/J.CHEMOSPHERE.2022.133688.
[27] S. Kundu, N. Karak, Polymeric photocatalytic membrane: an emerging solution for environmental remediation, Chem. Eng. J. 438 (2022) 135575, https://doi.org/10.1016/J.CEJ.2022.135575.
[28] M. Zeshan, I.A. Bhatti, M. Mohsin, M. Iqbal, N. Amjed, J. Nisar, N. AlMasoud, T. S. Alomar, Remediation of pesticides using TiO2 based photocatalytic strategies: a review, Chemosphere 300 (2022) 134525, https://doi.org/10.1016/J.CHEMOSPHERE.2022.134525.
[29] A. Talaiekhozani, S. Rezania, K.H. Kim, R. Sanaye, A.M. Amani, Recent advances in photocatalytic removal of organic and inorganic pollutants in air, J. Clean. Prod. 278 (2021) 123895, https://doi.org/10.1016/J.JCLEPRO.2020.123895.
[30] D. Castilla-Caballero, A. Hernandez-Ramirez, S. Vazquez-Rodriguez, J. Colina-Márquez, F. Machuca-Martínez, J. Barraza-Burgos, A. Roa-Espinosa, A. Medina-Guerrero, S. Gunasekaran, Effect of pyrolysis, impregnation, and calcination conditions on the physicochemical properties of TiO2/Biochar composites intended for photocatalytic applications, J. Environ. Chem. Eng. 11 (2023) 110274, https://doi.org/10.1016/j.jece.2023.110274.
[31] D. Castilla-Caballero, O. Sadak, J. Martínez-Díaz, V. Martínez-Castro, J. Colina-Márquez, F. Machuca-Martínez, A. Hernandez-Ramirez, S. Vazquez-Rodriguez, S. Gunasekaran, Solid-state photocatalysis for plastics abatement: a review, Mater. Sci. Semicond. Process 149 (2022) 106890, https://doi.org/10.1016/J.MSSP.2022.106890.
[32] W. Liang, Y. Luo, S. Song, X. Dong, X. Yu, High photocatalytic degradation activity of polyethylene containing polyacrylamide grafted TiO2, Polym. Degrad. Stab. 98 (2013) 1754–1761, https://doi.org/10.1016/j.polymdegradstab.2013.05.027.
[33] H. Wang, X. Li, X. Zhao, C. Li, X. Song, P. Zhang, P. Huo, A review on heterogeneous photocatalysis for environmental remediation: from semiconductors to modification strategies, Chin. J. Catal. 43 (2022) 178–214, https://doi.org/10.1016/S1872-2067(21)63910-4.
[34] X. Jiao, K. Zheng, Q. Chen, X. Li, Y. Li, W. Shao, J. Xu, J. Zhu, Y. Pan, Y. Sun, Y. Xie, Photocatalytic conversion of waste plastics into C2 fuels under simulated natural environment conditions, Angew. Chem. Int. Ed. 59 (2020) 15497–15501, https://doi.org/10.1002/ANIE.201915766.
[35] T. Uekert, H. Kasap, E. Reisner, Photoreforming of nonrecyclable plastic waste over a carbon nitride/nickel phosphide catalyst, J. Am. Chem. Soc. 141 (2019) 15201–15210, https://doi.org/10.1021/JACS.9B06872/SUPPL_FILE/JA9B06872_SI_001.PDF.
[36] T. Uekert, C.M. Pichler, T. Schubert, E. Reisner, Solar-driven reforming of solid waste for a sustainable future, 2020 4:5, Nat. Sustain. 4 (2020) 383–391, https://doi.org/10.1038/s41893-020-00650-x.

[37] D. Castilla-Caballero, A. Hernandez-Ramirez, S. Vazquez-Rodriguez, J. Colina-Márquez, F. Machuca-Martínez, J. Barraza-Burgos, A. Roa-Espinosa, A. Medina-Guerrero, S. Gunasekaran, Effect of pyrolysis, impregnation, and calcination conditions on the physicochemical properties of TiO2/Biochar composites intended for photocatalytic applications, J. Environ. Chem. Eng. 11 (2023) 110274, https://doi.org/10.1016/J.JECE.2023.110274.
[38] O. Das, D. Bhattacharyya, D. Hui, K.-T. Lau, Mechanical and flammability characterisations of biochar/polypropylene biocomposites, Compos B Eng. 106 (2016) 120–128, https://doi.org/10.1016/j.compositesb.2016.09.020.
[39] S. Kane, E. Van Roijen, C. Ryan, S. Miller, Reducing the environmental impacts of plastics while increasing strength: biochar fillers in biodegradable, recycled, and fossil-fuel derived plastics, Compos. Part C: Open Access 8 (2022) 100253, https://doi.org/10.1016/j.jcomc.2022.100253.
[40] W. Suliman, J.B. Harsh, N.I. Abu-Lail, A.-M. Fortuna, I. Dallmeyer, M. Garcia-Pérez, The role of biochar porosity and surface functionality in augmenting hydrologic properties of a sandy soil, Sci. Total Environ. 574 (2017) 139–147, https://doi.org/10.1016/j.scitotenv.2016.09.025.
[41] O. Das, A.K. Sarmah, The love-hate relationship of pyrolysis biochar and water: a perspective, Sci. Total Environ. 512–513 (2015) 682–685, https://doi.org/10.1016/j.scitotenv.2015.01.061.
[42] K.G. Roquemore, Hybrid designs for quadratic response surfaces, Technometrics 18 (1976) 419–423.
[43] J. Zolgharnein, M. Bagtash, N. Asanjarani, Hybrid central composite design approach for simultaneous optimization of removal of alizarin red S and indigo carmine dyes using cetyltrimethylammonium bromide-modified TiO2 nanoparticles, J. Environ. Chem. Eng. 2 (2014) 988–1000, https://doi.org/10.1016/j.jece.2014.03.017.
[44] D. Castilla-Caballero, J. Barraza-Burgos, S. Gunasekaran, A. Roa-Espinosa, J. Colina-Márquez, F. Machuca-Martínez, A. Hernández-Ramírez, S. Vázquez-Rodríguez, Experimental data on the production and characterization of biochars derived from coconut-shell wastes obtained from the Colombian Pacific Coast at low temperature pyrolysis, Data Brief. 28 (2020) 104855, https://doi.org/10.1016/J.DIB.2019.104855.
[45] Evonik Industries, AEROXIDE®, AERODISP® and AEROPERL® Titanium dioxide as photocatalyst, Tech. Inf. 1243 (2015).
[46] LyondellBasell, Pro-fax SG702-Product detail | LyondellBasell, (n.d.). ⟨https://www.lyondellbasell.com/en/polymers/p/Pro-fax-SG702/efbb8b3f-97b1-4bc3-9b66-317e06ef1d97⟩ (accessed July 20, 2020).
[47] K.A. Bustos-Torres, S. Vazquez-Rodriguez, A.M. de la Cruz, S. Sepulveda-Guzman, R. Benavides, R. Lopez-Gonzalez, L.M. Torres-Martínez, Influence of the morphology of ZnO nanomaterials on photooxidation of polypropylene/ZnO composites, Mater. Sci. Semicond. Process 68 (2017) 217–225, https://doi.org/10.1016/j.mssp.2017.06.023.
[48] K. Rajakumar, V. Sarasvathy, A. Thamarai Chelvan, R. Chitra, C.T. Vijayakumar, Natural weathering studies of polypropylene, J. Polym. Environ. 17 (2009) 191–202, https://doi.org/10.1007/s10924-009-0138-7.
[49] R.H. Myers, D.C. Montgomery, C.M. Anderson-Cook, Response Surface Methodology: Process and Product Optimization Using Designed Experiments, Wiley, 2016.
[50] J. Zolgharnein, M. Bagtash, N. Asanjarani, Hybrid central composite design approach for simultaneous optimization of removal of alizarin red S and indigo carmine dyes using cetyltrimethylammonium bromide-modified TiO2 nanoparticles, J. Environ. Chem. Eng. 2 (2014) 988–1000, https://doi.org/10.1016/j.jece.2014.03.017.
[51] C.-C. Mao, H.-S. Weng, Promoting effect of adding carbon black to TiO2 for aqueous photocatalytic degradation of methyl orange, Chem. Eng. J. 155 (2009) 744–749, https://doi.org/10.1016/j.cej.2009.09.016.
[52] T.S. Jamil, M.Y. Ghaly, N.A. Fathy, T.A. Abd El-Halim, L. Österlund, Enhancement of TiO2 behavior on photocatalytic oxidation of MO dye using TiO2/AC under visible irradiation and sunlight radiation, Sep Purif. Technol. 98 (2012) 270–279, https://doi.org/10.1016/j.seppur.2012.06.018.
[53] J. Brazard, T.B.M. Adachi, A. Turner, M. Filella, Determination of titanium speciation in consumer plastics by Raman microspectroscopy, Microchem. J. 208 (2025) 112391, https://doi.org/10.1016/J.MICROC.2024.112391.
[54] H. Wu, Y. Zhao, X. Dong, L. Su, K. Wang, D. Wang, Probing into the microstructural evolution of isotactic polypropylene during photo-oxidation degradation, Polym. Degrad. Stab. 183 (2021) 109434, https://doi.org/10.1016/J.POLYMDEGRADSTAB.2020.109434.
[55] M. Lu, X. Gao, P. Liu, H. Tang, F. Wang, Y. Ding, S. Zhang, M. Yang, Photo- and thermo-oxidative aging of polypropylene filled with surface modified fumed nanosilica, Compos. Commun. 3 (2017) 51–58, https://doi.org/10.1016/J.COCO.2017.02.004.
[56] J. Chen, L. Xia, M. Kong, Y. He, Y. Lv, Y. Huang, G. Li, Optimized design of environmentally-friendly polydopamine nanoparticles for the stabilization of both thermo- and photo-oxidation of polypropylene: size effects, Polym. Test. 116 (2022) 107795, https://doi.org/10.1016/J.POLYMERTESTING.2022.107795.
[57] K.A. Bustos Torres, Influencia de la morfología de ZnO en la fotooxidación de polipropileno, Tesis de maestría, Univ. Aut. ónoma De. Nuevo Le. óN. (2012). ⟨http://eprints.uanl.mx/2606/⟩.
[58] E. Andreassen, Infrared and Raman spectroscopy of polypropylene, in: Infrared and Raman spectroscopy of polypropylene, Springer, Dordrecht, 1999, pp. 320–328, https://doi.org/10.1007/978-94-011-4421-6_46.
[59] G. Kummerlöwe, B. Luy, Residual Dipolar Couplings for the Configurational and Conformational Analysis of Organic Molecules, Annu Rep. NMR Spectrosc. 68 (2009) 193–232, https://doi.org/10.1016/S0066-4103(09)06804-5.
[60] A. Prasert, S. Sontikaew, D. Sriprapai, S. Chuangchote, Polypropylene/ZnO nanocomposites: mechanical properties, photocatalytic dye degradation, and antibacterial property, Materials 13 (2020) 1–16.
[61] N.S. Allen, Photochemistry and photophysics of polymer materials, J. Wiley, 2010.
[62] O. Agboola, R. Sadiku, T. Mokrani, I. Amer, O. Imoru, Polyolefins and the environment, Polyolefin Fibres (2017) 89–133, https://doi.org/10.1016/B978-0-08-101132-4.00004-7.
[63] W. Suliman, J.B. Harsh, N.I. Abu-Lail, A.M. Fortuna, I. Dallmeyer, M. Garcia-Perez, Modification of biochar surface by air oxidation: Role of pyrolysis temperature, Biomass-.-. Bioenergy 85 (2016) 1–11, https://doi.org/10.1016/j.biombioe.2015.11.030.
[64] A.R. Zimmerman, Abiotic and microbial oxidation of laboratory-produced black carbon (biochar), Environ. Sci. Technol. 44 (2010) 1295–1301, https://doi.org/10.1021/es903140c.
[65] L. Zhou, C. Richard, C. Ferronato, J.M. Chovelon, M. Sleiman, Investigating the performance of biomass-derived biochars for the removal of gaseous ozone, adsorbed nitrate and aqueous bisphenol A, Chem. Eng. J. 334 (2018) 2098–2104, https://doi.org/10.1016/j.cej.2017.11.145.
[66] M. Smith, S. Ha, J.E. Amonette, I. Dallmeyer, M. Garcia-Perez, Enhancing cation exchange capacity of chars through ozonation, Biomass-.-. Bioenergy 81 (2015) 304–314, https://doi.org/10.1016/j.biombioe.2015.07.012.
[67] C. Chen, G. Levitin, D.W. Hess, T.F. Fuller, XPS investigation of Nafion® membrane degradation, J. Power Sources 169 (2007) 288–295, https://doi.org/10.1016/J.JPOWSOUR.2007.03.037.
[68] V. Rheinheimer, C. Unluer, J. Liu, S. Ruan, J. Pan, P.J.M. Monteiro, XPS Study on the Stability and Transformation of Hydrate and Carbonate Phases within MgO Systems, 2017, Vol. 10, Page 75, Materials 10 (2017) 75, https://doi.org/10.3390/MA10010075.
[69] H.L. Otálvaro-Marín, M.A. Mueses, F. Machuca-Martínez, Boundary layer of photon absorption applied to heterogeneous photocatalytic solar flat plate reactor design, Int. J. Photo 2014 (2014) 1–8, https://doi.org/10.1155/2014/930439.
[70] J. Lehmann, S. Joseph, Biochar Environ. Manag. (2009), https://doi.org/10.4324/9781849770552.
[71] L. Lu, R. Shan, Y. Shi, S. Wang, H. Yuan, A novel TiO2/biochar composite catalysts for photocatalytic degradation of methyl orange, Chemosphere 222 (2019) 391–398, https://doi.org/10.1016/j.chemosphere.2019.01.132.
[72] A. Kumar, G. Sharma, M. Naushad, A.H. Al-Muhtaseb, A. García-Peñas, G.T. Mola, C. Si, F.J. Stadler, Bio-inspired and biomaterials-based hybrid photocatalysts for environmental detoxification: a review, Chem. Eng. J. 382 (2020) 122937, https://doi.org/10.1016/j.cej.2019.122937.
[73] T. Fazal, A. Razzaq, F. Javed, A. Hafeez, N. Rashid, U.S. Amjad, M.S. Ur Rehman, A. Faisal, F. Rehman, Integrating adsorption and photocatalysis: a cost effective strategy for textile wastewater treatment using hybrid biochar-TiO2 composite, J. Hazard Mater. 390 (2020) 121623, https://doi.org/10.1016/j.jhazmat.2019.121623.
[74] R. Djellabi, B. Yang, Y. Wang, X. Cui, X. Zhao, Carbonaceous biomass-titania composites with Ti–O–C bonding bridge for efficient photocatalytic reduction of Cr (VI) under narrow visible light, Chem. Eng. J. 366 (2019) 172–180, https://doi.org/10.1016/j.cej.2019.02.035.
[75] N.S. Allen, N. Mahdjoub, V. Vishnyakov, P.J. Kelly, R.J. Kriek, The effect of crystalline phase (anatase, brookite and rutile) and size on the photocatalytic activity of calcined polymorphic titanium dioxide (TiO2), Polym. Degrad. Stab. 150 (2018) 31–36, https://doi.org/10.1016/j.polymdegradstab.2018.02.008.
[76] L. Lu, R. Shan, Y. Shi, S. Wang, H. Yuan, A novel TiO 2 /biochar composite catalysts for photocatalytic degradation of methyl orange, (2019). https://doi.org/10.1016/j.chemosphere.2019.01.132.
[77] J. Zhang, P. Zhou, J. Liu, J. Yu, New understanding of the difference of photocatalytic activity among anatase, rutile and brookite TiO2, Phys. Chem. Chem. Phys. 16 (2014) 20382–20386, https://doi.org/10.1039/C4CP02201G.
[78] H. Zhang, Z. Wang, R. Li, J. Guo, Y. Li, J. Zhu, X. Xie, TiO2 supported on reed straw biochar as an adsorptive and photocatalytic composite for the efficient degradation of sulfamethoxazole in aqueous matrices, Chemosphere 185 (2017) 351–360, https://doi.org/10.1016/j.chemosphere.2017.07.025.
[79] D. Castilla-Caballero, A. Hernandez-Ramirez, S. Vazquez-Rodriguez, J. Colina-Márquez, F. Machuca-Martínez, J. Barraza-Burgos, A. Roa-Espinosa, A. Medina-Guerrero, S. Gunasekaran, Effect of pyrolysis, impregnation, and calcination conditions on the physicochemical properties of TiO2/Biochar composites intended for photocatalytic applications, J. Environ. Chem. Eng. 11 (2023) 110274, https://doi.org/10.1016/j.jece.2023.110274.
[80] M. Inyang, B. Gao, L. Wu, Y. Yao, M. Zhang, L. Liu, Filtration of engineered nanoparticles in carbon-based fixed bed columns, Chem. Eng. J. 220 (2013) 221–227, https://doi.org/10.1016/j.cej.2013.01.054.
[81] D. Wang, W. Zhang, X. Hao, D. Zhou, Transport of biochar particles in saturated granular media: Effects of pyrolysis temperature and particle size, Environ. Sci. Technol. 47 (2013) 821–828, https://doi.org/10.1021/es303794d.
[82] C. Wu, L. Wang, D. Harbottle, J. Masliyah, Z. Xu, Studying bubble–particle interactions by zeta potential distribution analysis, J. Colloid Interface Sci. 449 (2015) 399–408, https://doi.org/10.1016/J.JCIS.2015.01.040.
[83] D. Angın, Eff. Pyrolysis Temp. Heat. rate biochar obtained Pyrolysis Safflower seed Press cake 128 (2013) 593–597, https://doi.org/10.1016/j.biortech.2012.10.150.
[84] R. Keey Liew, W. Lun Nam, M. Yee Chong, X. Yee Phang, M. Huan Su, P. Nai Yuh Yek, N. Ling Ma, C. Kui Cheng, C. Tung Chong, S. Shiung Lam, Oil palm waste: An abundant and promising feedstock for microwave pyrolysis conversion into good quality biochar with potential multi-applications, (2018). https://doi.org/10.1016/j.psep.2017.10.005.

[85] R.K. Liew, C. Chai, P. Nai, Y. Yek, X.Y. Phang, M.Y. Chong, W.L. Nam, M.H. Su, W. H. Lam, L. Ma, S.S. Lam, Innovative production of highly porous carbon for industrial effluent remediation via microwave vacuum pyrolysis plus sodium-potassium hydroxide mixture activation, (2019). https://doi.org/10.1016/j.jclepro.2018.10.214.

[86] M. Keiluweit, P.S. Nico, M. Johnson, M. Kleber, Dynamic molecular structure of plant biomass-derived black carbon (biochar), Environ. Sci. Technol. 44 (2010) 1247–1253, https://doi.org/10.1021/es9031419.

[87] K. Song, H. Zhang, Q. Wu, Z. Zhang, C. Zhou, Q. Zhang, T. Lei, Structure and thermal properties of tar from gasification of agricultural crop residue, J. Therm. Anal. Calor. 119 (2015) 27–35, https://doi.org/10.1007/s10973-014-4081-z.

[88] S.X. Zhao, N. Ta, X.D. Wang, Effect of temperature on the structural and physicochemical properties of biochar with apple tree branches as feedstock material, Energ. (Basel) 10 (2017), https://doi.org/10.3390/en10091293.

[89] M. Ahmad, S.S. Lee, X. Dou, D. Mohan, J.K. Sung, J.E. Yang, Y.S. Ok, Effects of pyrolysis temperature on soybean stover- and peanut shell-derived biochar properties and TCE adsorption in water, Bioresour. Technol. 118 (2012) 536–544, https://doi.org/10.1016/j.biortech.2012.05.042.

[90] S.E. Petersen, J.W. Dubis, The mixed block/event-related design, Neuroimage 62 (2012) 1177–1184, https://doi.org/10.1016/J.NEUROIMAGE.2011.09.084.

[91] M. Abou Rjeily, M. Chaghouri, C. Gennequin, E. Abi Aad, J.H. Randrianalisoa, Investigating co-production of syngas, biochar, and bio-oil from flax shives biomass by pyrolysis and in-line catalytic hybrid reforming, 2023 14:20, Biomass-.-. Convers. Biorefinery 14 (2023) 25599–25625, https://doi.org/10.1007/S13399-023-04614-X.

[92] O. Azeta, A.O. Ayeni, O. Agboola, F.B. Elehinafe, A review on the sustainable energy generation from the pyrolysis of coconut biomass, Sci. Afr. 13 (2021) e00909, https://doi.org/10.1016/J.SCIAF.2021.E00909.

[93] Innovations for climate-friendly chemical production, (n.d.). ⟨https://www.basf.com/ca/en/who-we-are/sustainability/we-produce-safely-and-efficiently/energy-and-climate-protection/carbon-management/innovations-for-a-climate-friendly-chemical-production⟩ (accessed January 15, 2025).

[94] Gestión de la energía en Cali - UAO Portal, (n.d.). ⟨https://www.uao.edu.co/ingenieria/gestion-de-la-energia-en-cali/⟩ (accessed January 21, 2025).

[95] L. Henan Doing Environmental Protection Technology Co., What's the energy cost of running tyre pyrolysis plant project?_pyrolysis plant project running cost_Waste Tire/Plastic Pyrolysis Plant, (n.d.). ⟨https://www.wastetireoil.com/Pyrolysis_faq/Pyrolysis_Plant/energy_cost_of_running_tyre_pyrolysis_plant_project_1346.html⟩ (accessed January 21, 2025).

[96] Electric Power Monthly - U.S. Energy Information Administration (EIA), (n.d.). ⟨https://www.eia.gov/electricity/monthly/epm_table_grapher.php?t=epmt_5_3⟩ (accessed January 21, 2025).

[97] A. Dyjakon, T. Noszczyk, M. Smędzik, The influence of torrefaction temperature on hydrophobic properties of waste biomass from food processing, 2019, Vol. 12, Page 4609, Energies 12 (2019) 4609, https://doi.org/10.3390/EN12244609.

[98] R.S. BAROT, M. Ayar, D.H.S. Beravala, Energy efficient and sustainable design and development of muffle furnace for melting alloys, SSRN Electron. J. (2019), https://doi.org/10.2139/SSRN.3462641.